ABCF ATPases Involved in Protein Synthesis, Ribosome Assembly and Antibiotic Resistance: Structural and Functional Diversification across the Tree of Life

Victoriia Murina[1,2,†], Marje Kasari[1,†], Hiraku Takada[1,2], Mariliis Hinnu[3], Chayan Kumar Saha[1], James W. Grimshaw[4], Takahiro Seki[5], Michael Reith[1], Marta Putriņš[3], Tanel Tenson[3], Henrik Strahl[4], Vasili Hauryliuk[1,2,3] and Gemma Catherine Atkinson[1]

*1 - **Department of Molecular Biology,** Umeå University, 901 87 Umeå, Sweden*
*2 - **Laboratory for Molecular Infection Medicine Sweden (MIMS),** Umeå University, 901 87 Umeå, Sweden*
*3 - **University of Tartu,** Institute of Technology, Nooruse 1, 50411 Tartu, Estonia*
*4 - **Centre for Bacterial Cell Biology,** Institute for Cell and Molecular Biosciences Newcastle University, Richardson Road, Newcastle upon Tyne, NE2 4AX, United Kingdom*
*5 - **Department of Applied Chemistry and Biotechnology,** Faculty of Engineering, Chiba University, 263-8522 Chiba, Japan*

***Correspondence to Gemma Catherine Atkinson:** gemma.atkinson@umu.se*
https://doi.org/10.1016/j.jmb.2018.12.013
Edited by Anthony Maxwell

Abstract

Within the larger ABC superfamily of ATPases, ABCF family members eEF3 in *Saccharomyces cerevisiae* and EttA in *Escherichia coli* have been found to function as ribosomal translation factors. Several other ABCFs including biochemically characterized VgaA, LsaA and MsrE confer resistance to antibiotics that target the peptidyl transferase center and exit tunnel of the ribosome. However, the diversity of ABCF subfamilies, the relationships among subfamilies and the evolution of antibiotic resistance (ARE) factors from other ABCFs have not been explored. To address this, we analyzed the presence of ABCFs and their domain architectures in 4505 genomes across the tree of life. We find 45 distinct subfamilies of ABCFs that are widespread across bacterial and eukaryotic phyla, suggesting that they were present in the last common ancestor of both. Surprisingly, currently known ARE ABCFs are not confined to a distinct lineage of the ABCF family tree, suggesting that ARE can readily evolve from other ABCF functions. Our data suggest that there are a number of previously unidentified ARE ABCFs in antibiotic producers and important human pathogens. We also find that ATPase-deficient mutants of all four *E. coli* ABCFs (EttA, YbiT, YheS and Uup) inhibit protein synthesis, indicative of their ribosomal function, and demonstrate a genetic interaction of ABCFs Uup and YheS with translational GTPase BipA involved in assembly of the 50S ribosome subunit. Finally, we show that the ribosome-binding resistance factor VmlR from *Bacillus subtilis* is localized to the cytoplasm, ruling out a role in antibiotic efflux.

Introduction

Protein biosynthesis—translation—is the reading and deciphering of information coded in genes to produce proteins. It is one of the most ancient and central cellular processes, and control of the various stages of translation is achieved via an intricate interplay of multiple molecular interactions. For many years, enzymatic control of the ribosomal cycle was thought to be mainly orchestrated by translational GTPases (trGTPases). That view of translation has been nuanced by the identification of multiple ATPases in the ABC superfamily that have important roles in translational regulation on the ribosome. The ABC protein eEF3 (eukaryotic Elongation Factor 3) is an essential factor for polypeptide elongation in *Saccharomyces cerevisiae* [1] with proposed roles in E-site tRNA release and ribosome recycling [2–4]. This fungi-specific translational ABC ATPase appeared to be an exception to the tenet that trGTPases are the

enzymatic rulers of the ribosome, until ABCE1 (also known as Rli1), a highly conserved protein in eukaryotes and archaea, was identified as another ribosome recycling factor [5–7].

The ABC ATPases together comprise one of the most ancient superfamilies of proteins, evolving well before the last common ancestor of life [8]. The superfamily contains members with wide varieties of functions but is best known for its membrane transporters [9]. Families of proteins within the ABC superfamily are named alphabetically ABCA to ABCH, following the nomenclature of the human proteins [10]. While most ABCs carry membrane-spanning domains, these are lacking in ABCE and ABCF families [11]. ABCF proteins of eukaryotes include eEF3 and also other ribosome-associated proteins: Gcn20 is involved in sensing starvation by the presence of uncharged tRNAs on the eukaryotic ribosome [12]; ABC50 (ABCF1) promotes translation initiation in eukaryotes [13], and both Arb1 (ABCF2) and New1 have been proposed to be involved in biogenesis of the eukaryotic ribosome [14,15]. Ribosome binding by ABCF proteins seemed to be limited to eukaryotes until the characterization of ABCF member EttA (energy-dependent translational throttle A) found in diverse bacteria. *Escherichia coli* EttA binds to the E-site of the ribosome where it is proposed to "throttle" the transition from initiation to the elongation stage of translation in response to change in the intercellular ATP/ADP ratio [16,17]. EttA is one of four *E. coli* ABCFs, the others being YheS, Uup and YbiT. None of the latter three have yet been shown to operate on the ribosome [16].

Bacterial ABCF family members have been found to confer resistance to ribosome-inhibiting antibiotics widely used in clinical practise, such as ketolides [18], lincosamides [19–22], macrolides [23,24], oxazolidinones [25], phenicols [25], pleuromutilins [22] and streptogramins A [22,26] and B [24]. These *a*ntibiotic *re*sistance (ARE) ABCFs have been identified in antibiotic-resistant clinical isolates of *Staphylococcus*, *Streptomyces* and *Enterococcus* among others [27]. This includes the so-called ESKAPE pathogens *Enterococcus faecium* and *Staphylococcus aureus* that contribute to a substantial proportion of hospital-acquired multidrug-resistant infections [28]. As some efflux pumps carry the ABC ATPase domain, it was originally thought that ARE ABCFs similarly confer resistance by expelling antibiotics. However, as they do not carry the necessary transmembrane domains, this is unlikely [29,30]. In support of this, it was recently shown that *S. aureus* ARE VgaA protects protein synthesis activity in cell lysates from antibiotic inhibition and that *Enterococcus faecalis* ARE LsaA promotes the release of radioactive lincomycin from *S. aureus* ribosomes [31]. Using a reconstituted biochemical system, we have shown that VgaA and LsaA directly protect the ribosome peptidyl transferase center (PTC) from antibiotics in an ATP-dependent manner [32]. Recent cryo-electron microscopy structures of AREs *Pseudomonas aeruginosa* MsrE and *Bacillus subtilis* VmlR on the ribosome show that, like EttA, these ABCFs bind to the E-site of the ribosome, with extended inter-ABC domain linkers protruding into the PTC [33,34]. The ARE ABCFs therefore appear to either physically interact with the drug to displace it from the ribosome or allosterically induce a change in conformation of the ribosome that ultimately leads to drug drop-off [35–37].

Here, we carry out an in-depth survey of the diversity of ABCFs across 4505 species with sequenced genomes. We find 45 groups (15 in eukaryotes and 30 in bacteria), including 7 groups of AREs. So-called EQ_2 mutations, double glutamic acid to glutamine substitutions in the two ATPase active sites of EttA, lock the enzyme on the ribosome in an ATP-bound conformation, inhibiting protein synthesis and cellular growth [16,17]. We have tested the effect of equivalent mutations in the other three *E. coli* ABCFs—YbiT, YheS and Uup—as well as the *B. subtilis* ARE VmlR. We establish genetic associations of *E. coli* ABCFs YheS and Uup with the translational GTPase BipA (also known as TypA) and through microscopy and polysome profile analyses confirm that VmlR does not confer lincomycin resistance through acting as a membrane-bound pump, but via direct interaction with cytoplasmic ribosomes.

Results

ABCFs are widespread among bacteria and eukaryotes

To identify candidate subfamilies of ABCFs and refine the classifications, an iterative bioinformatic protocol of sequence searching and phylogenetic analysis was applied. Sequence searching was carried out against a local database of 4505 genomes from across the tree of life. For an initial overview of the breadth of diversity of ABCFs across life, sequence searching began with a local BlastP search against a translated coding sequence database limited by taxonomy to one representative per class, or order if there was no listed class for that species in the NCBI taxonomy database. From phylogenetic analysis of the hits, preliminary groups were identified and extracted to make Hidden Markov Models (HMMs) for further sequence searching and classification. Additional sequences from known ARE ABCFs were included in phylogenetic analyses in order to identify groups of ARE-like ABCFs. HMM searching was carried out at the genus level followed by phylogenetic analysis to refine subfamily identification, with final predictions made at the species level. The resulting classification of 16,848 homologous sequences comprises 45 subfamilies, 15 in eukaryotes and 30 in bacteria. Phylogenetic

analysis of representatives across the diversity of ABCFs shows a roughly bipartite structure, with most eukaryotic sequences being excluded from those of bacteria with strong support (Fig. 1). Five eukaryotic groups that fall in the bacterial part of the tree are likely to be endosymbiotic in origin (see the section *Bacteria-like eukaryotic ABCFs*, below).

ABCFs are widespread among bacteria and eukaryotes; there are on average four ABCFs per bacterial genome and five per eukaryotic genome. However, there is considerable variation in how widespread each subfamily is (Table 1). The presence of all subfamilies in each genome considered here is shown in Table S1, with the full set of sequence identifiers and domain composition recorded in Table S2. Domain coordinates by amino acid position can be found in Table S3. Within bacteria, Actinobacteria, and Firmicutes are the phyla with the largest numbers of ABCFs (up to 11 per genome), due to expansions in ARE and potential novel ARE subfamilies. Among eukaryotes, plants and algae encode the most subfamilies, probably due in part to gene acquisition from endosymbiosis events. The diatom *Fragilariopsis cylindrus* has 30 ABCFs and the Haptophyte *Emiliania huxleyi* has 26. Bacterial contamination can sometimes inflate the number of genes in eukaryotic genomes as noted previously for trGTPases [35]. However, as all the *Fragilariopsis* and *Emiliania* sequences belong to typically eukaryotic subgroups, they do not appear to be the result of bacterial contamination. The Tibetan antelope *Pantholops hodgsonii*, on the other hand, has 25 ABCFs, 20 of which belong to bacterial subgroups. This genome is known to be contaminated by sequences from *Bradyrhizobium*, a well-known laboratory contaminant [41]. Thus, the bacteria-like hits from *P. hodgsonii* are most likely artifacts rather than bona fide cases of horizontal gene transfer from bacteria to eukaryotes.

The broad distribution and multi-copy nature of ABCFs suggests an importance of these proteins. However, they are not completely universal and are absent in almost all Archaea. The euryarcheaotes *Candidatus Methanomassiliicoccus intestinalis*, *Methanomethylophilus alvus*, *Methanomassiliicoccus luminyensis* and *Thermoplasmatales archaeon BRNA1* are the only archaeal genomes in which we identified ABCFs, in each case YdiF. However, with more archaeal genomes being completed, the complement of ABCFs found in isolated lineages of this domain of life is likely to increase. ABCFs are lacking in 214 bacterial species from various phyla, including many endosymbionts. However, the only phylum that is totally lacking ABCFs is Aquificae. ABCFs are almost universal in Eukaryotes; the only genomes where they were not detected are those of Basidomycete *Postia placenta*, Microsporidium *Enterocytozoon bieneusi*, and apicomplexan genera *Theileria*, *Babesia* and *Eimeria*.

Many of the phylogenetic relationships among subfamilies of ABCFs are poorly resolved (Fig. 1). This is not surprising, since these represent very deep bacterial relationships that predate the diversification of major phyla and include gene duplication, and differential diversification and loss, and likely combine both vertical inheritance and horizontal gene transfer. Although relationships cannot be resolved among all subfamilies, some deep relationships do have strong support [e.g., maximum likelihood bootstrap (MLB) percentage of more than 85%, ultrafast bootstrap (UFB) support of over 90%, and Bayesian inference posterior probability (BIPP) of 1.0]; EttA and Uup share a common ancestor to the exclusion of other ABCFs with full support (100% MLB, 100% UFB and 1.0 BIPP Figs. 1 and S1), and YheS is the closest bacterial group to the eukaryotic ABCFs with strong support (94% MLB, 98% UFB and 1.0 BIPP; Figs. 1 and S1, S1 Text). This latter observation suggests that eukaryotic-like ABCFs evolved from within the diversity of bacterial ABCFs. However, this depends on the root of the ABCF family tree. To address this, phylogenetic analysis was carried out of all ABCFs from *E. coli*, *Homo sapiens*, *S. cerevisiae* and *B. subtilis*, along with ABCE family sequences from the UniProt database [38]. Rooting with ABCE does not provide statistical support for a particular group at the base of the tree, but does support the eukaryotic subgroups being nested within bacteria, with YheS as the closest bacterial group to the eukaryotic types (Fig. 2). It also shows that eEF3 and New1 are nested within the rest of the ABCF family, thus confirming their identity as ABCFs, despite their unusual domain structure. To address the possibility that due to recombination the two ABC domains of the ABCF family may have had different evolutionary histories, we repeated our phylogenetic analysis of representative sequences with the ABC domains uncoupled and aligned to each other (Fig. 1, Test S1). With this very short alignment (204 positions) containing a larger proportion of almost invariant active site residues, there is even less statistical support for relationships among subgroups. Nevertheless, we still retain the branches that are well supported in our full-length analyses (Fig. 1), and thus, there is no evidence for recombination.

Domain architectures in the ABCF family are variable

To assess the conservation of domains across the family tree of ABCFs, we extracted the domain regions from subfamily alignments, made HMMs representing each domain region and scanned every sequence in our database. We find that the most common domain and subdomain arrangement is an N-terminal ABC1 nucleotide binding domain (NBD) containing an internal Arm subdomain (the L1-interacting region first reported for EttA [16,17]), followed by the Linker region joining to the ABC2 NBD (Fig. 3A). The inter-domain Linker (as it

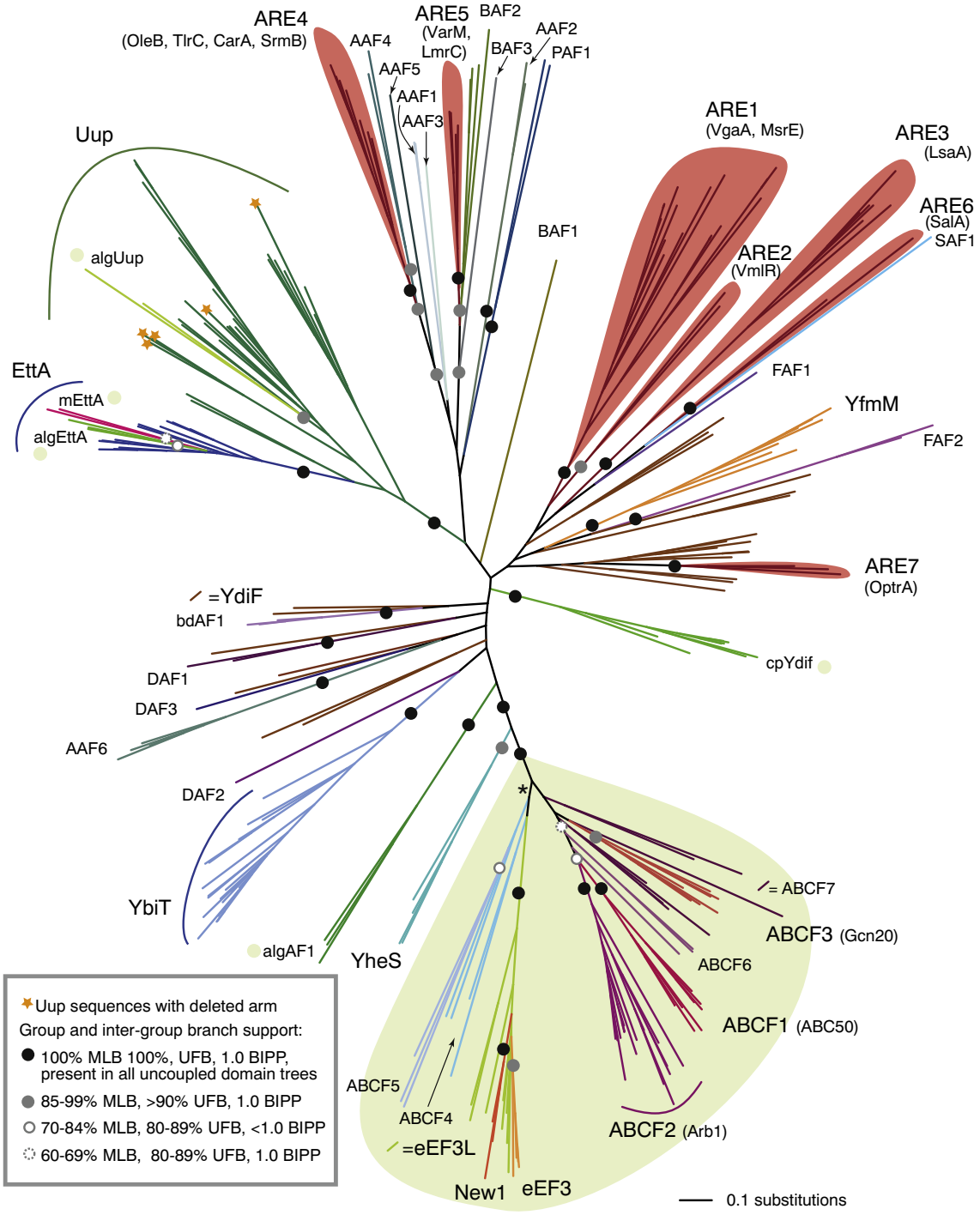

Fig. 1. The family tree of ABCFs has a bipartite structure corresponding to eukaryotic-like and bacterial (and organellar)-like sequences. The tree is a RaxML maximum likelihood phylogeny of representatives across the ABCF family with branch support values from 100 bootstrap replicates with RaxML (MLB), 1000 UFB replicates with IQ-TREE and BIPP. The inset box shows the legend for subfamily and intersubfamily support; support values within subfamilies and that are less that 60% MLB are not shown. Species were chosen that sample broadly across the tree of ABCF-encoding life, sampling at least one representative from each subfamily. Green shading shows the eukaryotic type ABCFs; other subgroups are bacterial unless marked with a green shaded circle to indicate eukaryotic groups with potentially endosymbiotic origin. CpYdif contains both cyanobacterial and predicted chloroplast sequences. The full tree with taxon names and sequence IDs is shown in Fig. S1. Branch lengths are proportional to amino acid substitutions as per the scale bar in the lower right. The asterisked branch is not supported by this data set; however, it is supported at 85% MLB in phylogenetic analysis of the eukaryotic subgroup and its viral relatives, rooted with YheS (Fig. S3).

Table 1. The subfamilies of the ABCF family, and the numbers (N) of phyla and species in which they are encoded

Subfamily	N Phyla	N Species	Notes on function, relationships and taxonomic distribution
YdiF	42	1852	Broad distribution in bacteria; polyphyletic
Uup[a]	24	3104	Broad distribution in bacteria; paraphyletic to EttA. Inc. P resistance TaeA [38]
EttA	18	2337	Broad distribution in bacteria; translation factor
YbiT	15	1874	Broad distribution in bacteria; potential translation factor
BAF2	7	305	Proteobacteria, Planctomycetes, Spirochaetes, Actinobacteria, Bacteroidetes, Gemmatimonadetes, Cyanobacteria
ARE1[a]	6	269	M, L, S, P, K resistance, inc. VgaA [21], MsrA [18], MsrE [33]; Firmicutes, Actinobacteria, Spirochaetes, Bacteroidetes, Proteobacteria, Tenericutes
ARE3[a]	5	261	L resistance inc. LsaA [20]; Firmicutes, Spirochaetes, Proteobacteria, Fusobacteria, Actinobacteria
DAF1	5	58	Spirochaetes, Proteobacteria, Deferribacteres, Fibrobacteres, Chlamydiae
YfmM	5	587	Firmicutes, Tenericutes, Proteobacteria, Fusobacteria, Bacteroidetes
YheS	5	1234	Proteobacteria, Bacteroidetes, Cyanobacteria, Arthropoda, Elusimicrobia
BAF3	4	111	Bacteroidetes, Proteobacteria, Cyanobacteria, Elusimicrobia
DAF2	4	24	Proteobacteria, Planctomycetes, Spirochaetes, Omnitrophica
ARE2[a]	2	54	Antibiotic resistance inc. VmlR [19]; Firmicutes, Tenericutes
ARE4[a]	2	173	M,M16 resistance inc. CarA [39], SrmB [39], TlrC [39], OleB [23]; Actinobacteria, Chloroflexi
ARE5[a]	2	408	L,S resistance inc. VarM [26], LmrC [40]; Actinobacteria, Proteobacteria
BAF1	2	20	Firmicutes, Actinobacteria
PAF1	1	138	Proteobacteria
AAF1	1	313	Actinobacteria
AAF2	1	301	Actinobacteria
AAF4	1	219	Actinobacteria
AAF6	1	649	Actinobacteria
AAF3	1	8	Actinobacteria
AAF5	1	25	Actinobacteria
ARE6[a]	1	8	L, S resistance SalA [22]; Firmicutes
ARE7[a]	1	35	Oxazolidinone resistance OptrA [25], Firmicutes
BdAF1	1	176	Bacteroidetes
DAF3	1	36	Proteobacteria
FAF1	1	37	Firmicutes
FAF2	1	42	Firmicutes
SAF1	1	66	Firmicutes
ABCF2	27	560	Arb1 ribosome biogenesis factor; broadly distributed but lacking in Apicomplexa and Microsporidia
ABCF1	23	376	ABC50 translation initiation factor; found in plants, diverse algae, and opisthokonts excluding fungi
ABCF7	16	131	Found in plants, diverse algae, Alveolata, Excavata and Microsporidia
ABCF3	13	382	Gcn20 starvation response; Opisthokonts
eEF3L	9	83	Diverse algae, Chytridiomycota and choanoflagellates
ABCF4	7	37	Diverse algae and Filozoa
ABCF5	7	105	Diverse algae and fungi
cpYdiF	7	85	Diverse algae
algAF1	6	25	Diverse algae
cpEttA	6	18	Chloroplast targeting peptides predicted; plants and diverse algae
algUup	5	17	Found in diverse algae
ABCF6	5	17	Found in diverse algae and Amoebozoa
mEttA	3	14	Mitochondrial targeting peptides predicted; diverse algae, Amoebozoa
New1	3	127	Fungi
eEF3	2	138	Translation factor; fungi

Resistance to antibiotic class in notes column is as follows: M, 14- and 15-membered ring macrolides; M16, 16-membered ring macrolides; L, lincosamides; S, streptogramins; K, ketolides; P, pleuromutilins.
[a] Subfamilies containing known AREs.

is referred to for VgaA [39] and MsrE [33]) corresponds to the structural region referred to as the P-site tRNA interaction motif, PtIM for EttA [16,17], and the ARE domain (ARD) for VmlR [34]. Variations on this basic structure include deletions in the Arm and Linker regions, insertion of a Chromo (chromatin organisation modifier) subdomain in the ABC2 NBD, and extension of N and C termini by sequence extensions (Fig. 3A). The domain structures of eukaryotic ABCFs are more diverse than those of bacteria, with greater capacity for extensions of the N-terminal regions to create new domains (Fig. 3A). An increased propensity to evolve extensions, especially at the N terminus is also seen with eukaryotic members of the trGTPase family [35]. In

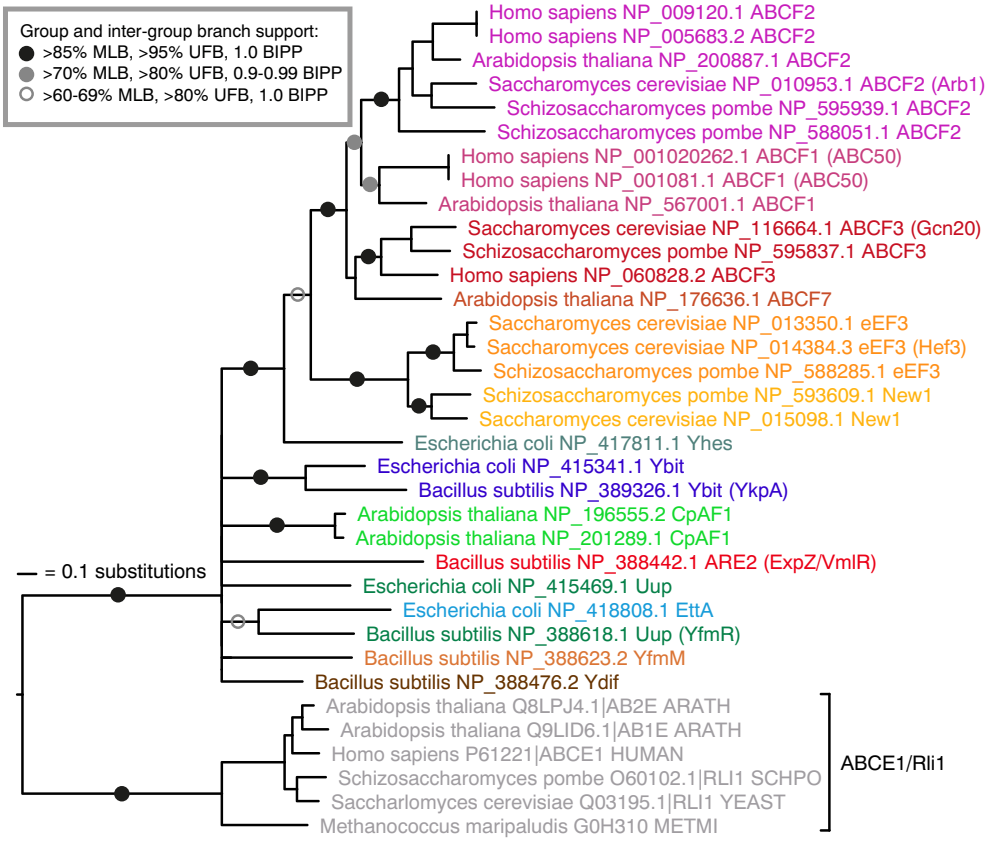

Fig. 2. Rooting with ABCE shows eukaryotic-like ABCFs nesting within bacterial-like ABCFs, with YheS as the sister group to the eukaryotic-like clade. Maximum likelihood phylogeny of representatives across the ABCF family, and ABCE sequences from the UniProt database. Branch support from 200 bootstrap replicates with RaxML (MBP), 1000 UFB replicates with IQ-TREE and BIPP is indicated with the key in the inset box. Branch lengths are proportional to amino acid substitutions as per the inset scale bar.

bacteria, terminal extensions of ABCFs tend to be at the C terminus (Fig. 3A–B).

Cryo-electron microscopy structures show that bacterial ABCFs bind to the same site of the ribosome, which is different from that of eEF3 [2,17,33,34], and this is reflected in their domain architectures. eEF3 carries additional N-terminal domains and does not have the Arm subdomain that in EttA binds the L1 stalk and ribosomal protein L1. Instead it carries a Chromo subdomain in the ABC2 NBD that—from a different orientation to the Arm domain of EttA—interacts with and stabilizes the conformation of the L1 stalk [2]. The Arm subdomain is also missing in eEF3-like close relatives New1 and eEF3L. Although the Arm is widespread in bacterial ABCFs, it is not universal; it is greatly reduced in a number of subfamilies, with the most drastic loss seen in ARE1 and 2 (Fig. 3A, and see the *Putative AREs* section, below). Subdomain composition can even vary within subfamilies; Uup has lost its arm independently in multiple lineages (Figs. 1 and S1).

Arms, Linkers and CTD extensions are poorly conserved at the primary sequence level but are similar in terms of composition, all being rich in charged amino acids, particularly arginine and lysine. Their variable presence and length suggests that they can be readily extended or reduced during evolution. The CTD of Uup forms a coiled coil structure that is capable of binding DNA [40]. However, whether DNA binding is its primary function is unclear. The CTD of YheS has significant sequence similarity (*E* value 3.58e−03) to the tRNA binding CTD of Valine-tRNA synthetase (NCBI conserved domains database accession cl11104). *In silico* coiled coil prediction suggests that there is a propensity of all these regions to form coiled coil structures (Fig. 3B). Extensions and truncations of the Arms, Linkers and CTD extensions possibly modulate the length of coiled coil protrusions that extend from the globular mass of the protein.

Eukaryotic ABCFs comprise 15 subfamilies

eEF3, New1 and eEF3L

eEF3, eEF3L and New1 group together and are particularly distinct members of the ABCF family. The

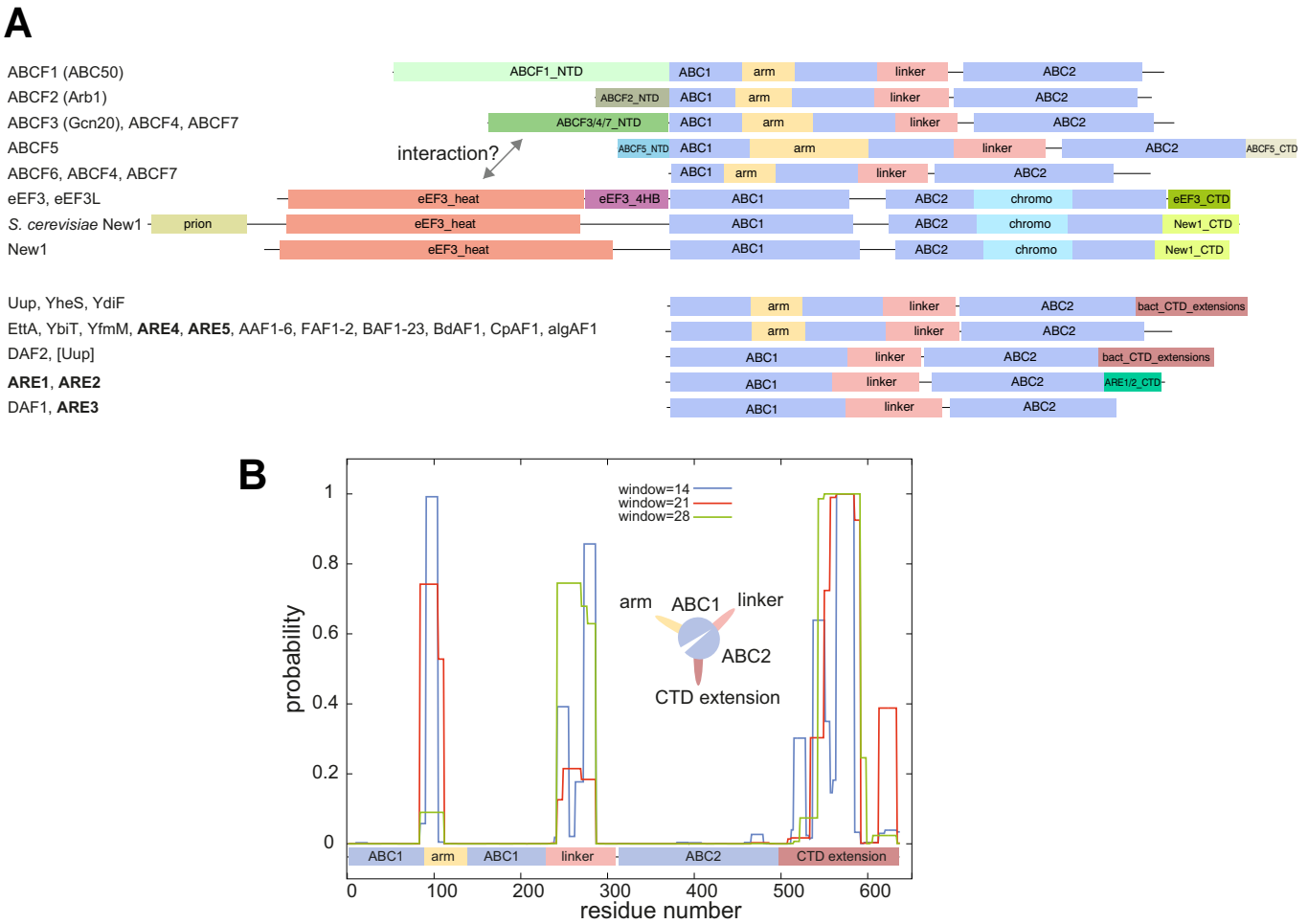

Fig. 3. Typical domain and subdomain architectures of ABCFs. (A) Boxes show domains as predicted by HMMs. Full coordinates and sequence data for these examples are recorded in Table S3. The gray arrow indicates possible interactions between the HEAT domain of eEF3/New1/eEF3L and the N-terminal domain of ABCF3, ABCF4 and ABCF7. (B) Predicted coiled coil regions of *E. coli* YheS along the protein length. Inset: cartoon representation of the coiled coil subdomains protruding from the core ABC domains.

eEF3 subfamily represents the classical fungal proteins, while eEF3L is a more divergent group found mainly in protists (see below). eEF3 has a recent paralogue in *S. cerevisiae* (Hef3 (Fig. 2), YEF3B) that apparently arose as a result of the whole genome duplication in yeast [42,43]. The conservation of domain structure in eEF3/New1/eEF3L suggests that they bind the ribosome similarly (Fig. 3A). Ribosome binding by eEF3 involves the Chromo subdomain, and the HEAT (*H*untington, *E*F3, *A* subunit of PP2A, *T*OR1) domain [2], which, in addition to New1 and eEF3L, is also found in the protein Gcn1, a binding partner of the ABCF Gcn20 [44] (see the section *ABCF1–7*, below). eEF3 has a distinct C-terminal extension (Fig. 3A), through which it interacts with eEF1A [45]. It has been suggested that this leads to the recruitment of eEF1A to *S. cerevisiae* ribosomes [45,46]. The New1 CTD contains a region of sequence similarity to the eEF3 CTD; both contain a polylysine/arginine-rich tract of 20–25 amino acids (Fig. S2). In *S. cerevisiae* eEF3, this is at positions 1009–1031, which falls within the eEF1A-binding site. Thus, eEF1A binding may be a common feature of eEF3, New1, and also eEF3L, which commonly includes an eEF3-like C-terminal extension (Table S2).

We find eEF3-like (eEF3L) factors in a range of eukaryotes including choanoflagellates, haptophytes, heterokonts, dinoflagellates, cryptophytes and red and green algae. This suggests that the progenitor of eEF3 was an ancient protein within eukaryotes and has been lost in a number of taxonomic lineages. Alternatively, eEF3L may have been horizontally transferred in eukaryotes. eEF3L is found in *Chlorella* viruses [47] and *Phaeocystis* viruses (Fig. S3), suggesting that this may be a medium of transfer. There is no "smoking gun" for viral-mediated transfer in the phylogenies, in that eukaryotic eEF3L sequences do not nest within viral sequence clades (Fig. S3). However, given the close association of viral and protist eEF3L, this still remains a possibility. Curiously, the taxonomic distribution of eEF3L in available genomes of diverse and distantly related protists is similar (although not identical) to that of the unusual elongation factor 1 (eEF1A) paralogue EFL [48] (Table S4). The propensity for eEF3/eEF3L/New1 to be present in EFL-encoding organisms and absent in eEF1A-encoding organisms is significant at the level of $P < 0.0001$ with Fisher's exact test. Yeasts are an exception to this tendency, in that they carry eEF1A and eEF3. Like eEF3L, EFL can be found in viruses such as *Aureococcus anophagefferens* virus (NCBI protein accession YP_009052194.1). As eEF3 interacts with eEF1A [46], the equivalents eEF3L and EFL may also interact in the organisms that encode them.

Like eEF3, New1 is found across the fungal tree of life (Table S1, Fig. S3). *S. cerevisiae* New1 has previously been reported to carry a prion-like Y/N/Q/G repetitive region in the N-terminal domain before the HEAT domain [49]. We find that this region is limited in taxonomic distribution to Saccharomycetale yeast (Table S2, Figs. 3A and S2). Thus, it is not found in the N-terminal region of *Schizosaccharomyces pombe* New1 (also known as Elf1).

ABCF1–7

ABCF1–7 comprise the "ancestral-type" eukaryotic ABCFs, in that they have the typical ABC domain structure that is seen in bacterial ABCFs, and they lack the Chromo and HEAT domains that are found in eEF3, New1 and eEF3L (Fig. 3A). All of the terminal extensions found in ABCF subfamilies are biased toward charged amino acids, often present as repeated motifs. The ABCF1 (ABC50) NTD (which interacts with eIF2 [50]) is, due to its length and number of repeats, one of the most striking (Fig. S2). It contains multiple tracts of poly-lysine/arginine, poly-glutamic acid/aspartic acid and—in animals—poly-glutamine. ABCF1 and ABCF2 have moderate support as sister groups (Fig. 1), and both have representatives in all eukaryotic superphyla, but are not universal. Lineages that have notable absences of ABCF1 are fungi, amoebozoa and most Aves (birds) (Tables 1 and S1). Schizosaccharomycetes carry a divergent ABCF1 NTD domain-containing protein (ABCF1/2) that associates phylogenetically with ABCF2 (Figs. S1 and S3).

ABCF2 (Arb1) is essential in yeast and its disruption leads to abnormal ribosome assembly [14]. Human ABCF2 can complement an Arb1 deletion, suggesting conservation of function [51]. The protein is broadly distributed across eukaryotes, with the notable exception of the *Alveolata* superphylum (Table S1). Like other ABCF terminal extensions, the ABCF2 N-terminal domain is rich in lysine, in this case lysine and alanine repeats.

In yeast, where it is known as Gcn20, ABCF3 is a component of the general amino acid control response to amino acid starvation, acting in a complex with Gcn1 [52]. Gcn20 binds to Gcn1 via the latter's HEAT-containing N-terminal domain [44], an interaction that is conserved in ABCF3 and Gcn1 of *Caenorhabditis elegans* [53]. As the HEAT domain is also found in eEF3, this raises the possibility that Gcn20/ABCF3 and eEF3 interact in encoding organisms (Fig. 3A). Possible support for this comes from the observation that eEF3 overexpression impairs Gcn2 activation [54].

ABCF3 is widespread in eukaryotes, but absent in heterkont algae and archaeplastida. However, these taxa encode ABCF4 and ABCF7 of unknown function, which have N-terminal domains homologous to ABCF3. Thus, ABCF4 and ABCF7 may be the functional equivalents of ABCF3 in these taxa, potentially interacting with HEAT domain-containing eEF3L in organisms that encode the latter (Fig. 3A). ABCF3 from four fungi (*Setosphaeria turcica*, NCBI protein accession number XP_008030281.1; *Cochliobolus sativus*, XP_007703000.1; *Bipolaris*

oryzae, XP_007692076.1; and *Pyrenophora teres*, XP_003306113.1) are fused to a protein with sequence similarity to WHI2, an activator of the yeast general stress response [55].

ABCF5 is a monophyletic subfamily limited to fungi and green algae (*Volvox* and *Chlamydomonas*), with a specific NTD and CTD (Figs. 1 and 2A). ABCF5 is found in a variety of Ascomycete and Basidiomycete fungi, including the yeast *Debaryomyces hansenii*, but is absent in yeasts *S. pombe* and *S. cerevisiae*. ABCF4 is a polyphyletic group of proteins found in various algal and amoeba protists that cannot be assigned to the ABCF5, or eEF3/eEF3L/New1 clades. In eukaryotic ABCF-specific phylogenetic analysis, ABCF4/ABCF5/eEF3/eEF3L/New1 are separated from all other eukaryotic ABCFs with moderate support (85% MLB Fig. S3). ABCF6 represents a collection of algal and amoebal sequences that associate with the ABCF1 + ABCF2 clade with mixed support in phylogenetic analysis (Fig. 1).

Bacterial-like eukaryotic ABCFs

Five eukaryotic subfamilies are found in the bacteria-like subtree: algAF1, algUup, mEttA, algEttA and cpYdiF (Fig. 1). Given their affiliation with bacterial groups, they may have entered the cell with an endosymbiotic ancestor. Indeed, chloroplast-targeting peptides are predicted at the N termini of the majority of cpYdiF sequences and mitochondrial localization

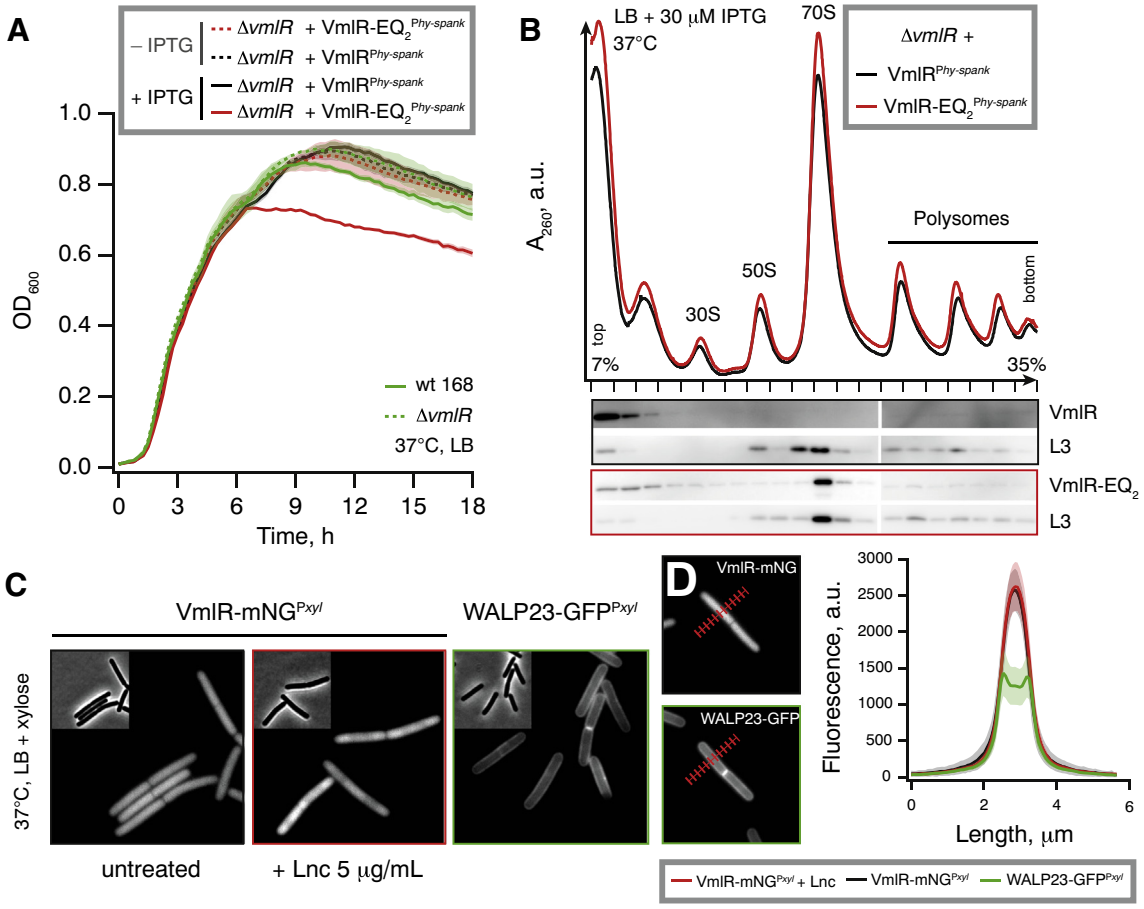

Fig. 4. *B. subtilis* ARE VmlR is a cytoplasmic protein that directly protects the ribosome from antibiotics. (A) Growth of wild-type *B. subtilis* 168, isogenic Δ*vmlR* knockout as well as Δ*vmlR* knockout expressing either wild-type or EQ_2 version of VmlR under the control of IPTG-inducible $P_{hy\text{-}spank}$ promoter. Six biological replicates were averaged for each growth curve and the data presented as geometric means ± standard deviation. (B) Polysome analysis and Western blotting of Δ*vmlR B. subtilis* expressing C-terminally HTF-tagged wild-type and EQ_2 version of VmlR. (C) Phase contrast and fluorescence images of uninhibited *B. subtilis* cells expressing VmlR-mNeonGreen (VmlR-mNG) in the presence and absence of lincomycin (40-min incubation with 5 μg/mL) and a model transmembrane protein WALP23-GFP are shown for comparison. (D) Fluorescence intensity profiles were measured perpendicular to the cell length axis along a 325-nm-wide and 5.8-μm-long line as indicated. Fluorescence intensity profiles of cells expressing WALP23-GFP [62] and cells expressing VmlR-mNG in the presence and absence of lincomycin. The graph depicts the average fluorescence intensity profiles and the corresponding standard deviations (n = 30).

peptides at most mEttA N termini. The situation is less clear for the three remaining groups, with a mix of signal peptides, or none at all being predicted across the group members (Table S5).

Bacterial ABCFs comprise 30 subfamilies, most of which have unknown function

There are 30 groups of bacterial ABCFs, the most broadly distributed being YdiF (the subfamily is given the name of the *B. subtilis* protein as it is not present in *E. coli*) (Table 1). This subfamily is a paraphyletic grouping comprising ABCF sequences that cannot confidently be classified into any of the other subgroups (Fig. 1). The next most broadly distributed group is Uup (*B. subtilis* protein name YfmR), which itself is paraphyletic to EttA. *B. subtilis* does not encode EttA, but does encode YbiT (*B. subtilis* name YkpA). It also encodes two ABCFs not present in *E. coli*: YfmM and VmlR (also known as ExpZ). VmlR is in the ARE2 subfamily and confers resistance to virginiamycin M1 and lincomycin [19]. Insertional disruptants of all the chromosomal ABCF genes in *B. subtilis* strain 168 have been examined for resistance to a panel of nine MLS class antibiotics, and only VmlR showed any hypersensitivity [19]. With the exception of EttA [16,17] and the seven ARE ABCFs (Table 1), the biological roles of the other 22 bacterial ABCFs are largely obscure.

B. subtilis ARE VmlR is a cytoplasmic protein that directly protects the ribosome from antibiotics

B. subtilis virginiamycin M and lincomycin resistance factor ABCF VmlR was originally annotated as an ABC efflux transporter, that is, a membrane protein [19,56]. To probe VmlR's interaction with ribosomes in the cell, we took advantage of ATPase-deficient VmlR mutants generated by simultaneous mutation of both glutamate residues for glutamine (EQ_2) [57] that lock ABC enzymes in an ATP-bound active conformation [17,58]. In parallel to the current study, these mutations have allowed us to resolve the structure of VmlR on the ribosome [34]. In the case of EttA, expression of the EQ_2 mutant results in a dominant-negative phenotype as EttA incapable of ATP hydrolysis acts as a potent inhibitor of protein synthesis and, consequently, bacterial growth [16]. We constructed C-terminally tagged His_6-TEV-3xFLAG-tagged (HTF-tagged) wild-type and EQ_2 (*vmlR*-HTF and *vmlR*EQ_2-HTF) under the control of an IPTG-inducible $P_{hy\text{-}spank}$ promoter [59]. To probe the intracellular localization of VmlR, we C-terminally tagged VmlR with the mNeonGreen fluorescent protein [60] under the control of xylose inducible promoter protein P_{xyl} [61]. We have validated the functionality of the fusion constructs by lincomycin resistance assays using a Δ*vmlR* knock-out strain as a negative control and a Δ*vmlR* knock-out strain expressing untagged VmlR under the control of an IPTG-inducible $P_{hy\text{-}spank}$ promoter as a positive control (Fig. S4A–C). While C-terminal tagging with either HTF or mNeonGreen does not abolish VmlR's activity, the EQ_2 versions of the tagged proteins are unable to protect from lincomycin (Fig. S4B).

After establishing the functionality of the tagged VmlR constructs, we tested the effects of expression of either wild-type or EQ_2 VmlR-HTF on *B. subtilis* growth in rich LB media (Fig. 4A). Expression of the wild-type protein in the Δ*vmlR* background has no detectable effect. In contrast, the EQ_2 version inhibits growth: while exponential growth is unaffected, the cells enter the stationary phase at lower cell densities, abruptly stopping growth instead of slowing down gradually (Fig. 4A). Two factors are likely to cause the growth-phase specificity of the inhibitory effect. First, during the exponential growth cells efficiently dilute the toxic protein via cell division, and when the growth slows down, VmlR-EQ_2-HTF accumulates. Second, upon entering the early stationary phase, *B. subtilis* sequesters 70S ribosomes into inactive 100S dimers [63], and this decrease of active ribosome concentration could conceivably render the cells more vulnerable to the inhibitory effects of VmlR-EQ_2. We probed the interaction of wild-type and EQ_2 VmlR-HTF with ribosomes using polysome analysis in sucrose gradients in combination with Western blotting (Fig. 4B). While the wild-type protein barely enters the gradient (most likely dissociating from the ribosomes during centrifugation), the EQ_2 version almost exclusively co-localizes with the 70S peak fraction and is absent from the polysomal fractions (Fig. 4B), suggesting co-sedimentation of a tight 70S:VmlR-EQ_2 complex, and that VmlR-EQ_2 is incompatible with actively translating ribosomes.

Finally, having ascertained the functionality of VmlR-mNeonGreen (Fig. S4C), we imaged *B. subtilis* cells expressing VmlR-mNeonGreen in the presence and absence of lincomycin (Fig. 4C) and quantified the intensity of the fluorescent signal across the cell (Fig. 4D). As a positive control for membrane localization we used WALP23-GFP [62], an artificial model transmembrane helix WALP23 [64] fused with an N-terminal GFP label. We observe no evidence for association of VmlR with the membrane: the protein is clearly cytoplasmic, with a slight exclusion from the nucleoid in the presence of 5 μg/mL lincomycin. A likely explanation for this effect is the nucleoid compaction caused by inhibition of translation resulting in protein exclusion from the nucleoid-occupied space [65–67]. However, we cannot rule out that this general effect is potentiated by specific interaction of VmlR with strongly nucleoid-excluded ribosomes.

E. coli ABCFs EttA, YbiT, YheS and Uup interact genetically and functionally with protein synthesis and ribosome assembly

E. coli encodes four ABCFs: EttA, YbiT, YheS and Uup. An array of structural, biochemical and

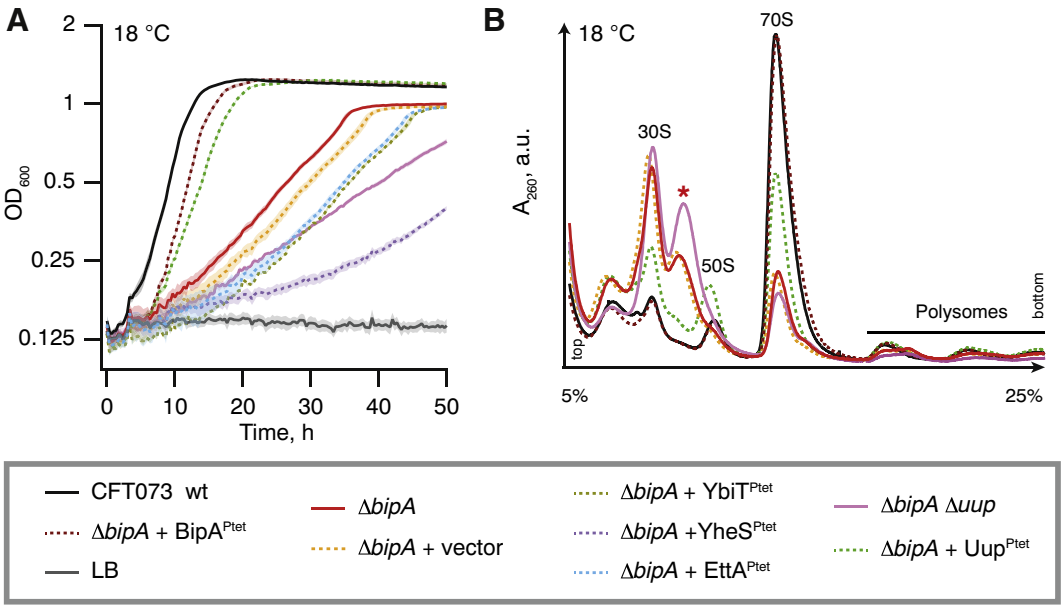

Fig. 5. Overexpression of *E. coli* ABCF Uup suppresses cold sensitivity and ribosome assembly defects caused by loss of translational GTPase BipA. Growth (A) and sucrose gradient polysome analysis (B) of CFT073 wild-type, isogenic Δ*bipA* and Δ*bipA*Δ*uup*, as well as CFT073 Δ*bipA* transformed with low-copy pSC vector expressing either BipA or ABCFs EttA, Uup, YheS and YbiT under control of constitutive promoter P_{tet}. All experiments were performed in filtered LB at 18 °C, and data are presented as geometric means ± standard deviation (n = 3).

microbiological methods has been used to establish that EttA operates on the ribosome [16,17]. Ribosomal association of the other *E. coli* ABCFs has not been shown. However, a recent PhD thesis by Dr. Katharyn L. Cochrane suggests that Uup interacts genetically with an enigmatic ribosome-associated factor, the trGTPase BipA (synonym TypA) [68]. The *E. coli bipA* knock-out strain is characterized by a decreased level of 50S subunits accompanied by an accumulation of pre-50S particles [69]. In the presence of its native substrate, GTP, BipA associates with mature 70S ribosomes [70], occupying the ribosomal A-site [71]. However, in the presence of the stress alarmone (p)ppGpp—a molecular mediator of the stringent response [72]—BipA binds the 30S subunit [73].

We have set out to systematically probe the involvement of *E. coli* ABCFs in protein synthesis. We used two experimental systems. The first is geared toward low level constitutive expression of native, untagged wild-type and EQ_2 proteins in a clinically relevant uropathogenic *E. coli* strain CFT073 [74]. For this, we cloned ABCF genes into a low copy pSC101 vector under control of a constitutive tet-promoter (P_{tet}) that in the original plasmid drives expression of the tetracycline efflux pump TcR [75]. Using the λRed-mediated gene disruption method [76], we generated a set of mutants lacking each of the four ABCF genes, as well as a Δ*bipA* and Δ*bipA*Δ*uup* knock-out strains. The second system allows inducible high-level expression of tagged proteins in the avirulent BW25113 *E. coli* strain [77,78]. We used wild-type and EQ_2 mutants of EttA, YbiT, YheS and Uup with N-terminal FLAG-TEV-His_6 (FTH)-tags expressed from a low copy pBAD18 plasmid under an arabinose-inducible araBAD (P_{BAD}) promoter. The BW25113 strain cannot metabolize arabinose (Δ*(araD–araB)567* genotype) [77], and therefore, the inducer is not metabolized during the experiment.

First, we tested the genetic interactions between *bipA* and all *E. coli* ABCFs in CFT073 background. At 37 °C the *bipA* CFT073 knock-out strain has no growth defect (Fig. S5A); however, at 18 °C, the Δ*bipA* strain displays a pronounced growth defect characteristic of strains defective in ribosome assembly (Fig. 5A) [79]. Ectopic expression of Uup efficiently suppresses the growth defect, while deletion of *uup* in the *bipA* background exacerbates it (Fig. 5A). Expression of EttA and Ybit has no effect, but expression of YheS leads to a dramatic growth defect. Importantly, in the wild-type background, the expression of YheS has no effect on growth at 18 °C (Fig. S5B), indicating that the genetic interaction between *bipA* and *yheS* is specific. As reported previously, disruption of *bipA* leads to a dramatic ribosome assembly defect at low (18 °C) temperature [69] (Fig. 5B). The levels of mature 70S ribosomes as well as 50S subunits are dramatically decreased, accompanied by an accumulation of 50S assembly precursors (the peak marked with an asterisk) and free 30S subunits. Ectopic expression of Uup partially suppresses these defects, and in the

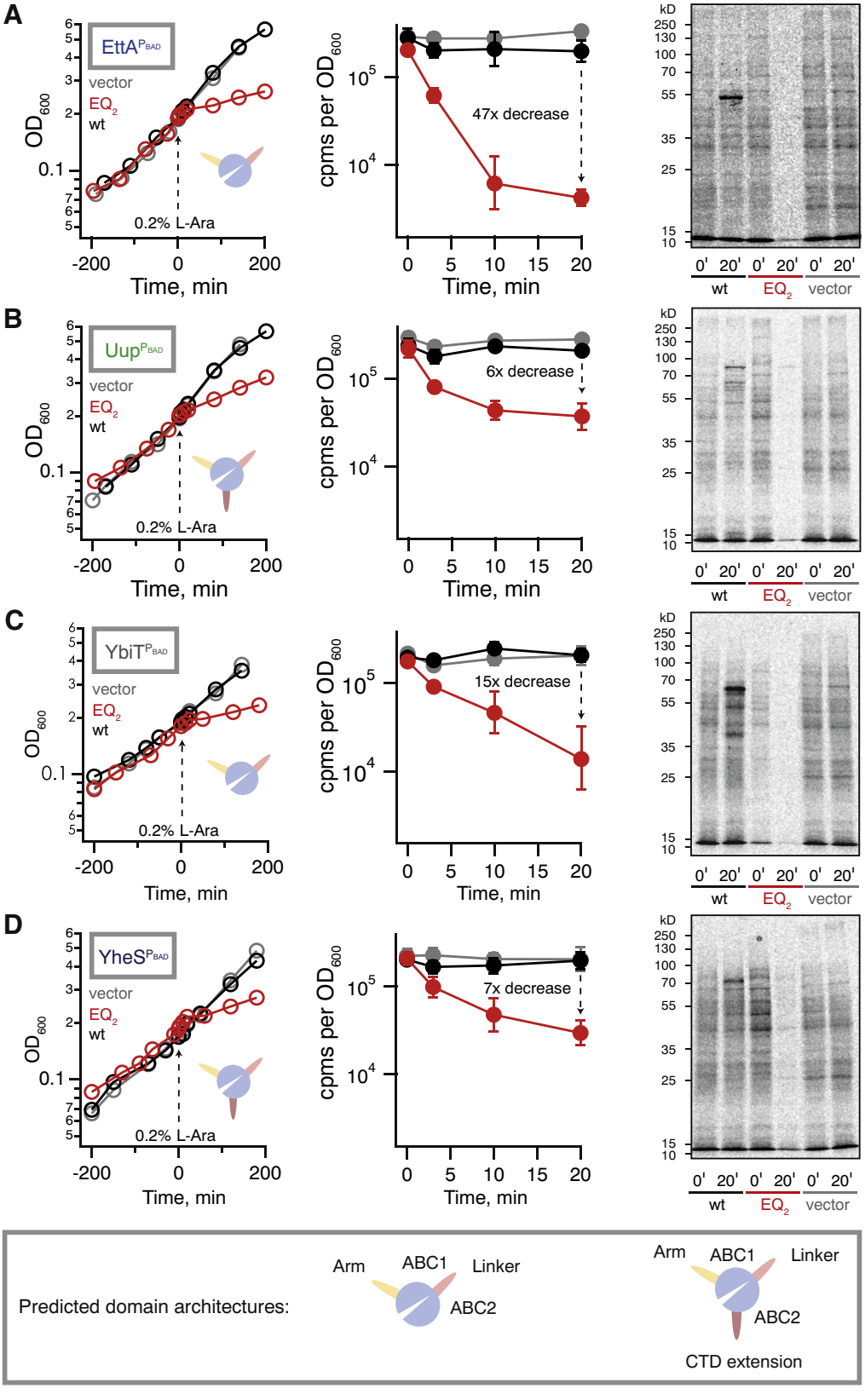

Fig. 6 (*legend on next page*)

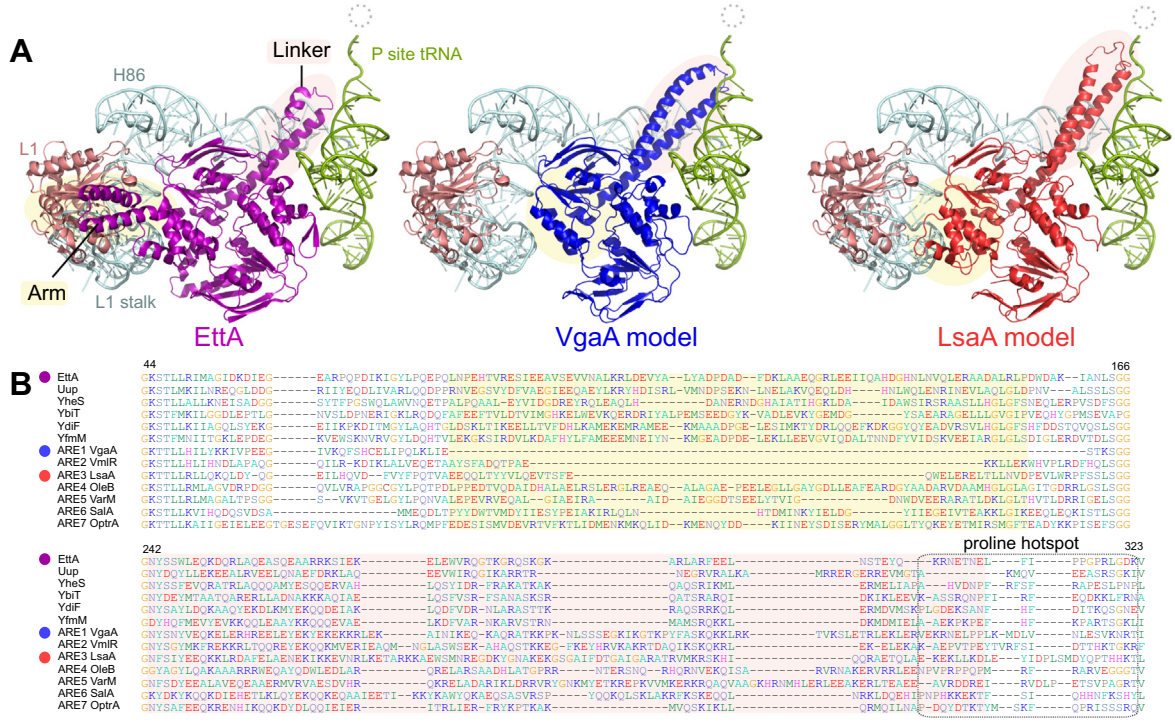

Fig. 7. AREs tend to have relatively long linker regions that potentially extend toward the ribosome bound antibiotics. (A) The structure of EttA and its interacting ribosomal components from PDB 3J5S [17] is shown alongside homology models of *S. aureus* VgaA and *E. faecalis* LsaA, using 3J5S as the template, with *de novo* modeling of the linker regions. The dotted circle shows the relative location of PTC-inhibiting antibiotics. Arm and linker regions are shaded in yellow and pink, respectively. (B) Extracts from the multiple sequence alignment of *E. coli* and *B. subtilis* ABCFs, and representative AREs, containing the Arm (yellow shading) and Linker (turquoise shading) subdomains. Alignment numbering is according to the EttA sequence. A boxed region shows a region that is particularly rich in proline and polyproline in various ABCF family members.

Δ*bipA*Δ*uup* strain, the defects are exacerbated. All of the effects described above are conditional on disruption of *bipA* since neither disruption of individual ABCF genes nor simultaneous disruption of *uup* and *ettA*—the only well-characterized ribosome-associated *E. coli* ABCF to date—causes cold sensitivity (Fig. S5C) or affects polysome profiles (Fig. S5D).

Next we set out to test the effects of EQ_2 versions of ABCFs on translation. We validated the expression of the FTH-tagged ABCFs using Western blotting (Fig. S6A). As was observed for untagged Uup (Fig. 5A), the expression of FTH-tagged Uup suppresses the cold sensitivity caused by *bipA* deletion, while YheS expression exacerbates the growth defect (Fig. S6B–C). Expression of the EQ_2 versions universally causes growth inhibition, both at 18 °C in Δ*bipA* CFT073 (Fig. S6C) and at 37 °C in the wild-type BW25113 background (Fig. 6). Overexpression of none of the wild-type ABCFs results in a growth defect (Fig. 6A–D). Next, we used a ^{35}S-methionine pulse-labeling assay as a readout of translational inhibition. For all the ABCF-EQ_2s, the

Fig. 6. Expression of *E. coli* ABCF-EQ_2 mutants inhibits growth and protein synthesis. Growth of wild-type *E. coli* BW2513 transformed with pBAD18 vector (gray trace) as well as *E. coli* BW2513 expressing either wild-type (black trace) or EQ_2 mutants (red trace) of EttA (A), Uup (B), YbiT (C), and YheS (D) under the control of arabinose-inducible promoter P_{BAD}. Radiographs show the effect of wild-type and EQ_2 ABCF expression on protein synthesis, as probed by pulse labeling with L-[^{35}S]-methionine. Expression was induced by the addition of L-arabinose to a final concentration of 0.2% at time point 0, and efficiency of incorporation was quantified by scintillation counting and visualized by autoradiography at 0- and 20-min time points. Scintillation counting data are presented as geometric means ± standard deviation (n = 3). All experiments were performed at 37 °C in Neidhardt MOPS medium [80] supplemented with 0.4% glycerol as a carbon source. The inset cartoons are a representation of ABCF domains and sub-domains, as per the legend in the lower box.

methionine incorporation decreases, showing that protein synthesis is clearly inhibited. The strongest effect is observed for EttA-EQ_2 (Fig. 6A) and YbiT-EQ_2 (Fig. 6C), and the weakest is seen for Uup-EQ_2 (Fig. 6B).

Phylogenetic analysis reveals putative AREs

Through phylogenetic analysis of predicted proteins and previously documented AREs with sequences available in UniProt [38] and the Comprehensive Antibiotic Resistance Database (CARD) [81], we have identified seven groups of AREs (Fig. 1, Table 1). Surprisingly, these can be quite variable in their subdomain architecture (Fig. 7A). Some AREs (ARE1–5) have experienced extension of the Linker by on average around 30 amino acids compared to EttA, which is in line with the observation that the extended Linkers of ARE1 MsrE and ARE2 VmlR are in close contact with the bound antibiotic [33,34]. However, Linker extension is not the rule for AREs; ARE7 (OptrA) has a Linker of comparable length to the *E. coli* ABCFs (Fig. 7A). This supports the notion based on the VmlR–ribosome co-structure that antibiotic protection by ABCFs involves allosteric changes in the ribosome as well as direct protein–drug interaction [34]. The Arm subdomain that in EttA interacts with the L1 ribosomal protein and the L1 stalk rRNA (Fig. 7A) varies in length among AREs, and the CTD extension may or not be present (Fig. 7B). Surprisingly, the Uup protein from cave bacterium *Paenibacillus* sp. *LC231*, a sequence that is unremarkable among Uups (Fig. S1), confers resistance to the pleuromutilin antibiotic tiamulin when heterologously expressed in *E. coli* [82].

Actinobacteria are the source of many ribosome-targeting antibiotics [83], and they have evolved measures to protect their own ribosomes, including ARE4 (OleB) and ARE5 (VarM). In addition to these known AREs, Actinobacteria encode a number of other ABCFs specific to this phylum (AAF1–6; Table 1). It is possible that some—if not all—of these groups are in fact AREs. Other subfamilies may also be unidentified AREs, but two particularly strong candidates are BAF2 and BAF3 that have strong support for association with ARE5 (Fig. 1) and are found in a wide range of bacteria (Table 1). PAF1 is also worthy of investigation; it is found in the genomes of several pathogens in the proteobacterial genera *Vibrio*, *Enterobacter*, *Klebsiella*, *Serratia* and *Citrobacter*, but not *Escherichia* (Table S1). With the exception of antibiotic producers, known ARE ABCFs tend to have a variable presence within genera (Fig. S7), probably because they are frequently transferred on plasmids and other mobile elements (e.g., Refs. [25,84,85]). Therefore, variability in the presence of a subfamily across species in a genus can be an indication that an ABCF is an ARE. Taking into account phylogenetic relationships (Figs. 1 and S1) and disjunction within genera (Fig. S7), we predict the following novel AREs: AAF1–5 (which tend to be found in antibiotic producers), BAF1–3, FAF1–2, and PAF1.

ABCFs are polyproline-rich proteins

Curiously, we find that ABCFs from both bacteria and eukaryotes are often rich in polyproline sequences, which are known to cause ribosome slow-down or stalling during translation [86]. This stalling is alleviated by the elongation factor EF-P in bacteria [87,88], and indeed, EF-P is required for full expression of EttA, which contains two XPPX motifs [89]. Fifty-six percent of all the sequences in our ABCF database contain at least two consecutive prolines, compared to an overall 37% of all the proteins in the predicted proteomes considered here. There is a particularly proline-rich hotspot in the C-terminal part of the Linker (Fig. 7B), which can be up to nine consecutive prolines long in the case of Uup from *Novosphingobium aromaticivorans* (NCBI protein accession number WP_028641352.1). Arms and CTD extensions are also polyproline hotspots; PPP is a common motif in the Arm of EttA proteins, and polyprolines are frequent in YdiF, Uup and YheS CTD extensions. Prolines are rigid amino acids, and conceivably, their presence may support the tertiary structures of ABCFs, particularly the orientation of the subdomain coiled coils [90].

Discussion

Toward a general model for non-eEF3 ABCF function

In the case of ABCFs that act on the assembled ribosome during translation, the E-site should be vacant (i.e., not filled by an E-site tRNA) for the protein to bind. Specifically, this would be when the E-site has not yet received a tRNA (in the case of 70S initiation complex binding by EttA [16,17]), or when an empty tRNA has dissociated and not been replaced (during slow or stalled translation such as in the presence of an antibiotic, as in the case of AREs [33,34]). EttA has been proposed to promote the first peptide bond after initiation through modulation of the PTC conformation [16,17]; similarly, allosteric effects acting on the PTC have been observed for the ARE VmlR [34]. This structural modulation or stabilization could conceivably be a general function of ABCFs, with the specific ribosomal substrate differing depending on the stage of translation, assembly, or cellular conditions. Differences in subdomains would determine both what is sensed and the resulting signal. For instance the presence of the Arm would affect signal transmission between the PTC and the L1 protein and/or the L1 stalk.

Evolution of AREs

In order to determine ARE capabilities and track the transfer routes of resistance, it is critical to be able to annotate ARE genes in genomes. This requires discrimination of antibiotic genes from homologous genes from which resistance functions have evolved. At present, this is not straightforward for ARE ABCFs, as the distinction between potential translation and ARE factors is ambiguous. ARE ABCFs have been compared to the Tet family of ARE proteins that evolved from trGTPase EF-G to remove tetracycline from the ribosome [29]. However, the distinction between Tet proteins and EF-G is much more clear-cut, with Tet comprising a distinct lineage in the evolutionary history of trGTPases [35]. The surprising lack of a clear sequence signature for ARE in the ARE ABCFs suggests that ARE functions may evolve in multiple ways in ABCFs and that ABCFs closely related to AREs may have similar functions to the AREs, while not conferring resistance. For example, there are multiple small molecules that bind the PTC and exit tunnel [91], and conceivably, ABCFs could be involved in sensing such cases, removing the small molecule, or allowing translation of a subset of mRNAs to continue in its presence. Even macrolide antibiotics that target the exit tunnel do not abrogate protein synthesis entirely, but rather reshape the translational landscape [92,93].

Conclusion

ABCFs are stepping into the limelight as important translation, ribosome assembly and ARE factors. We have found that hydrolysis-incompetent EQ_2 mutants of all four *E. coli* ABCFs inhibit protein synthesis, suggesting that they all function on the ribosome. Overexpression of Uup suppresses both the cold sensitivity and the 50S ribosome assembly defect caused by the loss of translational GTPase BipA, suggesting that Uup is involved in the 50S ribosome subunit assembly, either directly or indirectly, for example, by fine-tuning expression of ribosomal proteins. ARE2 VmlR has joined the ranks of AREs confirmed to act on the ribosome, along with ARE3 LsaA, and ARE1s VgaA and MsrE. This, combined with the well-established ribosome association of eukaryotic ABCFs, suggests that ribosome binding is a general—perhaps ancestral—feature of ABCFs. However, the ABCF family is diverse, and even within subfamilies, there can be differences in subdomain architecture. More structures of different ABCFs along with biochemical and phenotypic data are required to make sense of how our observed sequence differences translate into functional specialization and molecular mechanisms of the various ABCF subfamilies. We have identified clusters of ARE ABCFs and predicted likely new AREs. Strikingly, the AREs do not form a clear monophyletic group, meaning that ARE-linked function has evolved multiple times independently from the ABCF diversity or that this is an innate ability of ABCFs, raising the possibility of a general role of ABCFs in ribosome-binding small-molecule sensing and signalling.

Methods

Sequence searching and classification

Predicted proteomes were downloaded from the NCBI genome FTP site (2nd December 2014). One representative was downloaded per species of bacteria (i.e., not every strain). Seven additional proteomes were downloaded from JGI (*Aplanochytrium kerguelense*, *Aurantiochytrium limacinum*, *F. cylindrus, Phytophthora capsici*, *Phytophthora cinnamomi*, *Pseudo-nitzschia multiseries*, and *Schizochytrium aggregatum*). Previously documented AREs were retrieved from UniProt [38] and the Comprehensive Antibiotic Resistance Database (CARD) [81]. Taxonomy was retrieved from NCBI, and curated manually where some ranks were not available.

An initial local BlastP search was carried out locally with BLAST + v 2.2.3 [94] against a proteome database limited by taxonomy to one representative per class or (order if there was no information on class from the NCBI taxonomy database) using EttA as the query. Subsequent sequence searching against the proteome collections used hmmsearch from HMMER 3.1b1, with HMMs made from multiple sequence alignments of subfamilies, as identified below. The *E* value threshold for hmmsearch was set to $1e^{-70}$, a value at which the subfamily models hit outside of the eukaryotic-like or bacterial-like ABCF bipartitions, ensuring complete coverage while not picking up sequences outside of the ABCF family.

Sequences were aligned with MAFFT v7.164b (default settings) and Maximum Likelihood phylogenetic analyses were carried out with RAxML-HPC v.8 [95] on the CIPRES Science Gateway v3 [96] using the LG model of substitution, after removing positions containing >50% gaps. Additional phylogenetic analyses of representative sequences were carried out as described in the section "phylogenetic analysis of representatives", below. Trees were visualized with FigTree v. 1.4.2 (http://tree.bio.ed.ac.uk/software/figtree/) and visually inspected to identify putative subfamilies that preferably satisfied the criteria of (1) containing mostly orthologues and (2) having at least moderate (>60% bootstrap support). These subfamilies were then isolated, aligned separately and used to make HMM models. Models were refined with subsequent rounds of searching and classification into subfamilies first by comparisons of the *E* values of

HMM hits, then by curating with phylogenetic analysis. After the final classification of all ABCF types in all predicted protein sequences using HMMER, some manual correction was still required. For example, cyanobacterial sequences always hit the chloroplast HMM with a more significant *E* value than the bacterial model, and eEF3/New1/eEF3L sequences could not be reliably discriminated using *E* value comparisons. Therefore, the final classification is a manually curated version of that generated from automatic predictions (Table S2). All sequence handling was carried out with bespoke Python scripts, and data were stored in a MySQL database (exported to Excel files for the supplementary material tables). Identification of EFL and eEF1A in predicted proteomes was carried out with HMMER, using the HMMs previously published for these trGTPases [35]. The *E* value cutoff was set to e^{-200}, lenient enough to match both eEF1A and EFL, with assignment to either protein subfamily made by *E* value comparisons as above.

Domain prediction

Domain HMMs were made from subalignments extracted from subfamily alignments. Partial and poorly aligned sequences were excluded from the alignments. All significant domain hits ($< E$ value $1e^{-3}$) for each ABCF sequence were stored in the MySQL database. Sequence logos of domains were created with Skylign [97]. Putative transit peptides for mitochondrial and plastid subcellular localization were predicted with the TargetP web server hosted at the Technical University of Denmark [98].

Phylogenetic analysis of representatives

For the representative tree of the ABCF family, taxa were selected from the ABCF database to sample broadly across the tree of life, including eukaryotic protistan phyla, while also covering all subfamilies of ABCFs. Sequences were aligned with MAFFT with the

Table 2. Strains and plasmids used in the study

Strain or plasmid	Description	Reference
Strains: *E. coli*		
BW	BW25113 *E. coli*	[81]
CFT073	Uropathogenic *E. coli* O6:K2H1	[77]
CFTuup	Δ*uup* (locus tag c1085)	This study
CFTettA	Δ*yjjK* (locus tag c5478)	This study
CFTyheS	Δ*yheS* (locus tag c4127)	This study
CFTybiT	Δ*ybiT* (locus tag c0906)	This study
CFTbipA	Δ*yihK* (locus tag c4820)	This study
CFTbipA_pUup	Δ*yihK* with pSC-uup	This study
Strains: B. subtilis		
B. subtilis 168	*trpC2*	[106]
VHB5	*trpC2* Δ*vmlR*	This study
VHB38	*trpC2* Δ*vmlR amyE*::P_{xyl}-*vmlR-mNeoGreen Spc*^{r}	This study
VHB44	*trpC2* Δ*vmlR thrC*::$P_{hy\text{-}spnak}$-*vmlR Kan*^{r}	This study
VHB45	*trpC2* Δ*vmlR thrC*::$P_{hy\text{-}spnak}$-*vmlREQ2 Kan*^{r}	This study
VHB91	*trpC2* Δ*vmlR thrC*::$P_{hy\text{-}spnak}$-*vmlR-HTF Kan*^{r}	This study
VHB92	*trpC2* Δ*vmlR thrC*::$P_{hy\text{-}spnak}$-*vmlREQ*$_2$*-HTF Kan*^{r}	This study
HS64	*trpC2 amyE*::P_{xyl}-*WALP23-gfp Spc*^{r}	[66]
Plasmids		
pKD4	λRed PCR template plasmid with Kan resistance cassette; Kan^r Amp^r	[79]
pKD13	λRed PCR template plasmid with Kan resistance cassette; Kan^r Amp^r	[79]
pKD46	λRed recombinase helper plasmid, temperature sensitive; Amp^r	[79]
pCP20	FLP recombinase encoding plasmid, temperature sensitive; Amp^r	[79]
pSC101	pSC101 empty vector; Kan^r	This study
pSC-ettA	Constitutive *ettA* overexpression plasmid; Kan^r	This study
pSC-uup	Constitutive *uup* overexpression plasmid; Kan^r	This study
pSC-yheS	Constitutive *yheS* overexpression plasmid; Kan^r	This study
pSC-ybiT	Constitutive *ybiT* overexpression plasmid; Kan^r	This study
pSC-bipA	Constitutive *bipA* overexpression plasmid; Kan^r	This study
pHT009	Integration plasmid; Kan^r Amp^{r}Kan^r	This study
pSG1154	Integration plasmid; Spc^r Amp^r	[64]
pSHP2	Integration plasmid; Spc^r Amp^r	This study
VHp62	pAPNC with vmlR-HTF in SalI/BamHI sites; Spc^r Amp^r	Laboratory stock
VHp66	pAPNC with vmlREQ$_2$-HTF in SalI/BamHI sites; Spc^r Amp^r	Laboratory stock
pHT009-vmlR	pHT009 with vmlREQ2; Kan^r Amp^r	This study
pHT009-vmlR-HTF	pHT009 with vmlR-HTF in HindIII/SphI site; Kan^r Amp^r	This study
pHT009-vmlREQ2-HTF	pHT009 with vmlREQ2-HTF in HindIII/SphI site; Kan^r Amp^r	This study
pSHP2-vmlR	pSHP2 with vmlR in ApaI/EcoRI site; Spc^r Amp^r	This study

L-ins-i strategy [99] and positions with >50% gaps, and several ambiguously aligned positions at the termini were removed. The resulting 249 sequences and 533 positions were subject to RAxML and IQ-TREE Maximum Likelihood phylogenetic analysis, both run on the CIPRES Science Gateway v3 [96]. RAxML was run with the LG substitution matrix, as favored by ProtTest 2.4 [100] and 100 bootstrap replicates. Bootstrapping with RaxML yields a value (MLB percentage) for how much of the input alignment supports a particular branch in the tree topology and therefore the reliability of that branch. These support values are indicated on branches in the tree figures. In the case of IQ-TREE, the most appropriate model was selected by the program during the run, which also favored the LG substitution matrix. IQ-TREE was run with its ultrafast bootstrapping approximation method to ascertain support values (UFB) for branches out of 1000 replicates [101]. To test whether our trees made with ABC domains separately are incompatible (as might indicate recombination), the RaxML and IQ-TREE analyses were repeated with a data set containing the ABC domains uncoupled from each other and aligned together. Alignments were prepared as above, to make a data set of 204 alignment positions from 525 taxa (Text S1).

Bayesian inference phylogenetic analysis was carried out with MrBayes v3.2.6, also on the CIPRES gateway. The analysis was run for 1 million generations, after which the standard deviation of split frequencies (SDSF) was 0.08. The mixed model setting was used for determining the amino acid substitution matrix, which converged on WAG. RAxML analysis with the WAG model showed no difference in topology for well-supported branches compared to the RAxML tree with the LG model. Branch support values in this case are posterior probabilities, shown on the tree figure as BIPPs, on a scale of 0 to 1, with increasing probability.

For the rooted tree with ABCE as the outgroup, all ABCFs were selected from *Arabidopsis thaliana*, *H. sapiens, E. coli, B. subtilis, S. cerevisiae, S. pombe*, along with ABCE from these organisms and *Methanococcus maripaludis*. Ambiguously aligned sites were identified and removed manually. RAxML, IQ-TREE and MrBayes were carried out as above on the resulting 344 positions from 35 sequences. The MrBayes analysis stopped automatically when the SDSF dropped to the 0.009 threshold, which was at 235,000 generations.

For the tree of eukaryotic and viral ABCFs rooted with YheS, sequences were extracted from the ABCF database, and viral sequences were found in the NCBI protein database using BlastP. The resulting 658 sequences were aligned with MAFFT, and a RAxML analysis of 645 positions was carried out as above. The alignments used to build the phylogenies presented in the main text as supplementary information are available in Text S1, along with trees that are used for ascertaining branch support but not included as figures.

Structural analyses

Homology modeling of VgaA and LsaA was carried out using Swiss Model [102] with EttA (PDB ID 3J5S) as the template structure. Because the Linkers were lacking secondary structure, QUARK [103] was used for *ab initio* structure modeling of these regions, and the resulting coils were aligned back to the homology model using the structural alignment method of MacPyMOL [104]. The presence of coiled coil regions was predicted with the COILS program hosted at the ExPASy Bioinformatics Research Portal [105].

Construction of plasmids and bacterial strains

All bacterial strains and plasmids used in this study are described in Supplementary Methods and listed in Table 2.

Growth assays

Bacterial growth (OD_{600}) was monitored using a Bioscreen C (Oy Growth Curves Ab Ltd) microplate reader in Honeycomb plates (150 µL culture per well) with continuous shaking (speed: fast, amplitude: normal). All experiments with CFT073 were performed at 18 °C unless stated otherwise. Three biological replicates were averaged for each growth curve and the data presented as geometric means ± standard deviation.

E. coli transformed with pSC101-based expression plasmids

Overnight (16 h) cultures were pre-grown in LB medium supplemented with 50 µg/mL kanamycin, diluted to OD_{600} of 0.03 in filtered LB and grown in Bioscreen C microplate reader as described above.

E. coli transformed with pBAD-based expression plasmids

Overnight (16 h) cultures were pre-grown in Neidhardt MOPS medium [80] supplemented with 0.1% of casamino acids, 0.4% glucose as a carbon source and 100 µg/mL carbenicillin, diluted to OD_{600} of 0.03 in the same media but containing 0.5% glycerol instead of 0.4% glucose as well as supplemented with 0.5% arabinose and grown in Bioscreen C microplate reader as described above.

Antibiotic resistance testing of tagged B. subtilis VmlR

B. subtilis strains VHB38, VHB91 and VHB92 were pre-grown on LB plates overnight at 30 °C.

Fresh individual colonies were used to inoculate filtered LB medium, either in the presence and absence of 1 mM IPTG (for VHB91 and VHB92) or in the presence and absence of 0.3% xylose (for VHB38), and OD_{600} adjusted to 0.01. The cultures were seeded on Honeycomb plates, and plates incubated in a Bioscreen C at 37 °C with continuous shaking as described above for *E. coli* cultures. After 90-min incubation ($OD_{600} \approx 0.1$), increasing concentrations of lincomycin (final concentration 0–5 μg/mL) were added and growth was monitored for additional 6 h. Three biological replicates were averaged for each growth curve and the data presented as geometric means ± standard deviation.

Fluorescence microscopy

Fluorescence microscopy was carried out with cells grown to early-mid logarithmic growth phase (OD_{600} of 0.2–0.5) in LB medium at 37 °C in the presence or absence of inducers. The used inducer concentrations were 0.3% for VmlR-mNG and 1% for WALP23-GFP. If indicated, the cells were incubated with 5 μg/mL lincomycin upon shaking at 37 °C prior to the microscopy. The cells were immobilized on microscopy slides covered with a thin film of 1.2% (w/v) agarose in H_2O as described in detail elsewhere [107]. The microscopy was carried out with Nikon Eclipse Ti equipped with Nikon Plan Apo 100x/1.40 Oil Ph3 objective, Sutter Instrument Company Lambda LS xenon arc light source, and Photometrics Prime sCMOS camera. The images were captured using Metamorph 7.7 (Molecular Devices) and analyzed using Fiji [106].

Western blot analysis of FTH-tagged wt and EQ_2 *E. coli* ABCF proteins

Preparation of bacterial samples

Bacteria were grown either at 37 °C (*E. coli* BW25113 derivatives) or 18 °C (*E. coli ΔbipA* CFT073 derivatives) up to OD_{600} of 0.5 in 50 mL of Neidhardt MOPS minimal medium [80] supplemented with 0.1% casamino acids (w/v), 0.5% glycerol (w/v) and 100 μg/mL carbenicillin and L-arabinose was added to a final concentration of 0.2% (w/v). Cultures grown at 37 °C were harvested 10 min after induction by pouring them into precooled centrifuge bottles containing 100 g of crushed ice and centrifuged at 10,000 rpm for 10 min at 4 °C (Beckman JLA16.250 rotor). Cultures grown at 18 °C were harvested 5 h after induction by collecting into precooled centrifuge bottles and pelleting at 10,000 rpm for 10 min at 4 °C (Beckman JA25.50 rotor). Lysates were prepared the same as for polysome profiling of *E. coli* (see below).

Western blotting

Three micrograms of total protein as determined by Bradford assay of each sample was resolved on 10% SDS-PAGE gel and transferred to 0.2 μm nitrocellulose membrane (Trans-Blot® Turbo™ Transfer Pack, Bio-Rad) using Turbo MIXED MW protocol in Trans-Blot® Turbo™ Transfer System (Bio-Rad). The membrane was blocked in PBS-T (1× PBS 0.05% Tween-20) with 5% w/v nonfat dry milk at room temperature for 1 h. Antibody incubations were performed for 1 h in 1% nonfat dry milk in PBS-T with five 5-min washes in fresh PBS-T between and after antibody incubations. FTH-tagged ABCFs were detected using anti-Flag M2 primary (Sigma-Aldrich, F1804; 1:10,000 dilution) antibodies combined with anti-mouse-HRP secondary (Rockland; 610-103-040; 1:10,000 dilution) antibodies. ECL detection was performed on ImageQuant LAS 4000 (GE Healthcare) imaging system using Pierce® ECL Western blotting substrate (Thermo Scientific).

Polysome profiling analysis of *E. coli* strains

Preparation of bacterial samples

Overnight (16 h) cultures were pre-grown at 37 °C in LB medium supplemented with 50 μg/mL kanamycin in the case of strains transformed with pSC101-based expression plasmids. Overnight cultures were diluted in filtered LB (33 mL cultures) and after 24 h growth at 18 °C harvested by pouring into precooled centrifuge bottles and pelleting at 10,000 rpm for 10 min at 4 °C (Beckman JA25.50 rotor). For the sake of convenience, cultures were diluted to different starting densities (Table S3) to ensure that all of them reach $OD_{600} \approx 0.5$ simultaneously.

Preparation of clarified lysates

Cell pellets were resuspended in 0.4 mL of Polymix buffer [108] [20 mM HEPES–KOH (pH 7.5), 95 mM KCl, 5 mM NH_4Cl, 5 mM $Mg(OAc)_2$, 0.5 mM $CaCl_2$, 8 mM putrescine, 1 mM spermidine, 1 mM DTT] and 200 μL of pre-chilled zirconium beads (0.1 mm) were added to each sample. Cellular lysates were prepared by a FastPrep homogeniser (MP Biomedicals) (three 20 s pulses at speed 6.0 mp/s with chilling on ice for 1 min between the cycles) and clarified by centrifugation at 21,000*g* for 10 min at 4 °C. The supernatant was carefully collected avoiding the lipid layer and cellular pellet, aliquoted, frozen in liquid nitrogen and stored at −80 °C until further processing.

Sucrose gradient centrifugation

After melting the frozen samples on ice, 2 A_{260} units of each extract was loaded onto 5%–25% (w/v) sucrose

density gradients in Polymix buffer, 5 mM Mg^{2+} [108]. Gradients were resolved at 35,000 rpm for 2.5 h at 4 °C in SW41 rotor (Beckman) and analyzed using Biocomp Gradient Station (BioComp Instruments) with A_{260} as a readout. The ribosome profiles presented were normalized to the total area under the curve and are representative of at least three independent experiments for each strain.

Polysome profiling and Western blot analysis of *B. subtilis* strains

Experiments were performed as described above for *E. coli* strains, with minor modifications.

Preparation of bacterial samples and preparation of clarified lysates

VHB90 and VHB91 strains were pre-grown on LB plates overnight at 30 °C. Fresh individual colonies were used to inoculate 200 mL LB cultures. The cultures were grown at 37 °C until OD_{600} of 0.3 and IPTG was added to final concentration of 30 μM. After 30 min, cells were collected by centrifugation (8000 rmp, 10 min), dissolved in 0.5 mL of Polymix buffer [108] [20 mM HEPES–KOH (pH 7.5), 95 mM KCl, 5 mM NH_4Cl, 10 mM $Mg(OAc)_2$, 0.5 mM $CaCl_2$, 8 mM putrescine, 1 mM spermidine, 1 mM DTT, 2 mM PMSF], lysed (FastPrep homogeniser (MP Biomedicals): four 20 s pulses at speed 6.0 mp/s with chilling on ice for 1 min between the cycles) and clarified by ultracentrifugation (14,800 rpm, 20 min).

Sucrose gradient centrifugation and Western blotting

Clarified cell lysates were loaded onto 7%–35% sucrose gradients in Polymix buffer [108] [20 mM HEPES–KOH (pH) 7.5, 95 mM KCl, 5 mM NH_4Cl, 10 mM $Mg(OAc)_2$, 0.5 mM $CaCl_2$, 8 mM putrescine, 1 mM spermidine, 1 mM DTT] and subjected to centrifugation (35,000 rpm for 3 h at 4 °C). C-terminally HTF-tagged VmlR (wild-type and EQ_2 mutant) and ribosomal protein L3 of the 50S ribosomal subunit were detected using either anti-Flag M2 primary combined with anti-mouse-HRP secondary antibodies or anti-L3 primary (a gift from Fujio Kawamura) combined with goat anti-rabbit IgG-HRP secondary antibodies, respectively. All antibodies were used at 1:10,000 dilution.

L-[^{35}S]-methionine pulse labeling

Preparation of bacterial samples

Since glucose specifically inhibits the arabinose promoter, the cultures were grown in defined Neidhardt MOPS medium [80] supplemented with 0.4% glycerol as a carbon source. One colony of freshly transformed *E. coli* BW25113 cells expressing N-terminal FTH-tagged ABCFs (wild-type and EQ_2 mutants) from pBad vector was used to inoculate 10 mL of 1 × MOPS media supplemented with 0.4% glycerol 100 μg/mL carbenicillin, and the cultures were grown until early stationary phase (about 24 h). Stationary phase cells were diluted to OD_{600} of 0.04–0.07 in 25 mL of the same media, grown at 37 °C with vigorous shaking (200 rpm) to OD_{600} of 0.15–0.2 and expression of ABCFs was induced by addition of L-arabinose to the final concentration of 0.2%.

L-[^{35}S]-methionine pulse labeling

For radioactive pulse labeling, 1 μCi L-[^{35}S]-methionine (500 μCi, PerkinElmer) aliquots were prepared in 1.5 mL Eppendorf tubes. The specific activity of the radioactive methionine solution from PerkinElmer was 1175 Ci/mmol, and the working mix of "hot" and "cold" methionine with a final concentration of 15 mM had a specific activity of 205 mCi/mmol. As a zero time point, 1 mL of cell culture was taken and mixed with an aliquot of radioactive methionine just before inducing cells with L-arabinose. Simultaneously, a 1 mL aliquot was taken for an OD_{600} measurement. All consecutive samples were processed similarly at designated time points after induction. ^{35}S-methionine incorporation was stopped after 5 min by chloramphenicol added to the final concentration of 200 μg/mL. Subsequent processing of samples differs in the case of scintillation counting and autoradiography.

Scintillation counting

One milliliter of culture was combined with 200 μL of 50% trichloroacetic acid, passed through a GF/C filter (Whatman) prewashed with 5% trichloroacetic acid, and unincorporated label was removed by washing the filter with 5 mL of ice-cold 5% trichloroacetic acid followed by 5 mL of ice-cold 95% EtOH [109]. Filters were dried for at least 2 h and counted on a TRI-CARB 4910TR 110 V scintillation counter [PerkinElmer; 5 mL of ScintiSafe 3 scintillation cocktail (FisherScientific) per sample, pre-soaked with shaking for 15 min prior to counting].

Autoradiography

One milliliter-cultures were pelleted by centrifugation, and the cell pellet was washed with phosphate-buffered saline (PBS) to remove unincorporated L-[^{35}S]-methionine and dissolved/lysed in 50 μL 1 × SDS loading buffer. Samples were normalized by OD_{600} by addition of appropriate volume of 1 × SDS loading buffer (50–80 μL according to OD_{600}), and 10 μL of the sample was loaded onto 10% SDS-

PAGE and resolved electrophoretically (BioRad). Gels were dried on Whatman paper, exposed on BAS storage phosphor screen (GE Healthcare) overnight, and scanned by Typhoon imaging system (GE Healthcare).

Accession numbers

NCBI protein: YP_009052194.1; NCBI protein: XP_008030281.1; NCBI protein: XP_007703000.1; NCBI protein: XP_007692076.1; NCBI protein: XP_003306113.1; NCBI protein: WP_028641352.1; NCBI conserved domains database: cl11104.

Acknowledgments

We gratefully acknowledge Fujio Kawamura for providing anti-L3 primary antibodies and Stijn Hendrik Peeters for constructing the pSHP2 plasmid. Thanks to Martin Carr for discussion and advice about eEF3 and EFL co-distribution. This work was supported by the Swedish Research Council (2015-04746 to G.C.A. and 2017-03783 to V.H.), Ragnar Söderberg Foundation (V.H.), Umeå Centre for Microbial Research (UCMR) gender policy program (G.C.A.), Carl Tryggers grants CTS 14:34 and CTS 15:35 (G.C.A.), Kempe Stiftelse grant JCK-1627 (G.C.A.), Jeanssons Stiftelse grant (G.C.A.), Molecular Infection Medicine Sweden (MIMS) (V.H.), postdoctoral grant from Umeå Centre for Microbial Research (UCMR) (H.T.), BBSRC grant BB/M011186/1 (J.W.G. and H.S.), Umeå Universitet Insamlingsstiftelsen för medicinsk forskning (G.C.A. and V.H.), and the European Regional Development Fund through the Centre of Excellence for Molecular Cell Technology (V.H. and T.T.). The funders had no role in study design, data collection and analysis, decision to publish, or preparation of the manuscript.

Author Contributions: G.C.A. conceived the study and carried out all the bioinformatic analyses except for sequence logo construction and eEF1A/EFL/eEF3 co-distribution analysis, which was carried out by C.K. S. V.H., V.M., M.K., H.S., H.T., T.T. and M.P. designed experimental analyses. V.M., M.K., H.T., M.H., T.S., M. R., H.S. and J.W.G. carried out the experiments. V.H., G.C.A., H.S., T.T., H.T., V.M. and M.K. analyzed the data. G.C.A. and V.H. drafted the manuscript with input from V.M., M.K., H.T., M.H., C.K.S., J.W.G., T.S., M.P., T.T. and H.S.

Appendix A. Supplementary data

Supplementary data to this article can be found online at https://doi.org/10.1016/j.jmb.2018.12.013.

Received 7 November 2018;
Received in revised form 11 December 2018;
Accepted 15 December 2018
Available online 28 December 2018

Keywords:
ribosome;
translation;
antibiotic resistance;
ABCF;
ARE

†V.M. and M.K. contributed equally to this work.

Abbreviations used:
ARE, antibiotic resistance; PTC, peptidyl transferase center; HMMs, Hidden Markov Models; MLB, maximum likelihood bootstrap; UFB, ultrafast bootstrap; BIPP, Bayesian inference posterior probability; NBD, nucleotide binding domain.

References

[1] L. Skogerson, E. Wakatama, A ribosome-dependent GTPase from yeast distinct from elongation factor 2, Proc. Natl. Acad. Sci. U. S. A. 73 (1976) 73–76.
[2] C.B. Andersen, T. Becker, M. Blau, M. Anand, M. Halic, B. Balar, et al., Structure of eEF3 and the mechanism of transfer RNA release from the E-site, Nature 443 (2006) 663–668.
[3] S. Kurata, K.H. Nielsen, S.F. Mitchell, J.R. Lorsch, A. Kaji, H. Kaji, Ribosome recycling step in yeast cytoplasmic protein synthesis is catalyzed by eEF3 and ATP, Proc. Natl. Acad. Sci. U. S. A. 107 (2010) 10854–10859.
[4] F.J. Triana-Alonso, K. Chakraburtty, K.H. Nierhaus, The elongation factor 3 unique in higher fungi and essential for protein biosynthesis is an E site factor, J. Biol. Chem. 270 (1995) 20473–20478.
[5] A.V. Pisarev, M.A. Skabkin, V.P. Pisareva, O.V. Skabkina, A.M. Rakotondrafara, M.W. Hentze, et al., The role of ABCE1 in eukaryotic posttermination ribosomal recycling, Mol. Cell 37 (2010) 196–210.
[6] T. Becker, S. Franckenberg, S. Wickles, C.J. Shoemaker, A.M. Anger, J.P. Armache, et al., Structural basis of highly conserved ribosome recycling in eukaryotes and archaea, Nature 482 (2012) 501–506.
[7] D.J. Young, N.R. Guydosh, F. Zhang, A.G. Hinnebusch, R. Green, Rli1/ABCE1 recycles terminating ribosomes and controls translation reinitiation in 3′UTRs in vivo, Cell 162 (2015) 872–884.
[8] D. Caetano-Anolles, K.M. Kim, J.E. Mittenthal, G. Caetano-Anolles, Proteome evolution and the metabolic origins of translation and cellular life, J. Mol. Evol. 72 (2011) 14–33.
[9] A.L. Davidson, E. Dassa, C. Orelle, J. Chen, Structure, function, and evolution of bacterial ATP-binding cassette systems, Microbiol. Mol. Biol. Rev. 72 (2008) 317–364 (table of contents).
[10] M. Dean, A. Rzhetsky, R. Allikmets, The human ATP-binding cassette (ABC) transporter superfamily, Genome Res. 11 (2001) 1156–1166.
[11] I.D. Kerr, Sequence analysis of twin ATP binding cassette proteins involved in translational control, antibiotic

resistance, and ribonuclease L inhibition, Biochem. Biophys. Res. Commun. 315 (2004) 166–173.
[12] C.R. Vazquez de Aldana, M.J. Marton, A.G. Hinnebusch, GCN20, a novel ATP binding cassette protein, and GCN1 reside in a complex that mediates activation of the eIF-2 alpha kinase GCN2 in amino acid-starved cells, EMBO J. 14 (1995) 3184–3199.
[13] S. Paytubi, X. Wang, Y.W. Lam, L. Izquierdo, M.J. Hunter, E. Jan, et al., ABC50 promotes translation initiation in mammalian cells, J. Biol. Chem. 284 (2009) 24061–24073.
[14] J. Dong, R. Lai, J.L. Jennings, A.J. Link, A.G. Hinnebusch, The novel ATP-binding cassette protein ARB1 is a shuttling factor that stimulates 40S and 60S ribosome biogenesis, Mol. Cell. Biol. 25 (2005) 9859–9873.
[15] Z. Li, I. Lee, E. Moradi, N.J. Hung, A.W. Johnson, E.M. Marcotte, Rational extension of the ribosome biogenesis pathway using network-guided genetics, PLoS Biol. 7 (2009), e1000213.
[16] G. Boël, P.C. Smith, W. Ning, M.T. Englander, B. Chen, Y. Hashem, et al., The ABC-F protein EttA gates ribosome entry into the translation elongation cycle, Nat. Struct. Mol. Biol. 21 (2014) 143–151.
[17] B. Chen, G. Boel, Y. Hashem, W. Ning, J. Fei, C. Wang, et al., EttA regulates translation by binding the ribosomal E site and restricting ribosome-tRNA dynamics, Nat. Struct. Mol. Biol. 21 (2014) 152–159.
[18] E.D. Reynolds, J.H. Cove, Resistance to telithromycin is conferred by msr(A), msrC and msr(D) in *Staphylococcus aureus*, J. Antimicrob. Chemother. 56 (2005) 1179–1180.
[19] R. Ohki, K. Tateno, T. Takizawa, T. Aiso, M. Murata, Transcriptional termination control of a novel ABC transporter gene involved in antibiotic resistance in *Bacillus subtilis*, J. Bacteriol. 187 (2005) 5946–5954.
[20] K.V. Singh, G.M. Weinstock, B.E. Murray, An *Enterococcus faecalis* ABC homologue (Lsa) is required for the resistance of this species to clindamycin and quinupristin-dalfopristin, Antimicrob. Agents Chemother. 46 (2002) 1845–1850.
[21] G. Novotna, J. Janata, A new evolutionary variant of the streptogramin A resistance protein, Vga(A)LC, from *Staphylococcus haemolyticus* with shifted substrate specificity towards lincosamides, Antimicrob. Agents Chemother. 50 (2006) 4070–4076.
[22] C. Hot, N. Berthet, O. Chesneau, Characterization of sal(A), a novel gene responsible for lincosamide and streptogramin A resistance in *Staphylococcus sciuri*, Antimicrob. Agents Chemother. 58 (2014) 3335–3341.
[23] A. Buche, C. Mendez, J.A. Salas, Interaction between ATP, oleandomycin and the OleB ATP-binding cassette transporter of *Streptomyces antibioticus* involved in oleandomycin secretion, Biochem. J. 321 (Pt 1) (1997) 139–144.
[24] J.I. Ross, E.A. Eady, J.H. Cove, W.J. Cunliffe, S. Baumberg, J.C. Wootton, Inducible erythromycin resistance in staphylococci is encoded by a member of the ATP-binding transport super-gene family, Mol. Microbiol. 4 (1990) 1207–1214.
[25] Y. Wang, Y. Lv, J. Cai, S. Schwarz, L. Cui, Z. Hu, et al., A novel gene, optrA, that confers transferable resistance to oxazolidinones and phenicols and its presence in *Enterococcus faecalis* and *Enterococcus faecium* of human and animal origin, J. Antimicrob. Chemother. 70 (2015) 2182–2190.
[26] S. Kitani, T. Yamauchi, E. Fukushima, C.K. Lee, F. Ningsih, H. Kinoshita, et al., Characterization of varM encoding type II ABC transporter in *Streptomyces virginiae*, a Virginiamycin M1 producer, Actinomycetologica 24 (2010) 51–57.
[27] I.D. Kerr, E.D. Reynolds, J.H. Cove, ABC proteins and antibiotic drug resistance: is it all about transport? Biochem. Soc. Trans. 33 (2005) 1000–1002.
[28] L.B. Rice, Progress and challenges in implementing the research on ESKAPE pathogens, Infect. Control Hosp. Epidemiol. 31 (Suppl. 1) (2010) S7–10.
[29] D.N. Wilson, The ABC of ribosome-related antibiotic resistance, MBio 7 (2016).
[30] L.K.R. Sharkey, A.J. O'Neill, Antibiotic resistance ABC-F proteins: bringing target protection into the limelight, ACS Infect. Dis. 4 (2018) 239–246.
[31] L.K. Sharkey, T.A. Edwards, A.J. O'Neill, ABC-F Proteins Mediate Antibiotic Resistance through Ribosomal Protection, MBio 7 (2016).
[32] V. Murina, M. Kasari, V. Hauryliuk, G.C. Atkinson, Antibiotic resistance ABCF proteins reset the peptidyl transferase centre of the ribosome to counter translational arrest, Nucleic Acids Res. 46 (2018) 3753–3763.
[33] W. Su, V. Kumar, Y. Ding, R. Ero, A. Serra, B.S.T. Lee, et al., Ribosome protection by antibiotic resistance ATP-binding cassette protein, Proc. Natl. Acad. Sci. U. S. A. 115 (2018) 5157–5162.
[34] C. Crowe-McAuliffe, M. Graf, P. Huter, H. Takada, M. Abdelshahid, J. Novacek, et al., Structural basis for antibiotic resistance mediated by the *Bacillus subtilis* ABCF ATPase VmlR, Proc. Natl. Acad. Sci. U. S. A. 115 (36) (2018) 8978–8983.
[35] G.C. Atkinson, The evolutionary and functional diversity of classical and lesser-known cytoplasmic and organellar translational GTPases across the tree of life, BMC Genomics 16 (2015) 78.
[36] A. Donhofer, S. Franckenberg, S. Wickles, O. Berninghausen, R. Beckmann, D.N. Wilson, Structural basis for TetM-mediated tetracycline resistance, Proc. Natl. Acad. Sci. U. S. A. 109 (2012) 16900–16905.
[37] W. Li, G.C. Atkinson, N.S. Thakor, U. Allas, C.C. Lu, K.Y. Chan, et al., Mechanism of tetracycline resistance by ribosomal protection protein Tet(O), Nat. Commun. 4 (2013) 1477.
[38] The UniProt Consortium, UniProt: the universal protein knowledgebase, Nucleic Acids Res. 45 (2017) D158-D69.
[39] J. Lenart, V. Vimberg, L. Vesela, J. Janata, G. Balikova Novotna, Detailed mutational analysis of vga(a) interdomain linker: implication for antibiotic resistance specificity and mechanism, Antimicrob. Agents Chemother. 59 (2015) 1360–1364.
[40] . L. Carlier, A.S. Haase, M.Y. Burgos Zepeda, E. Dassa, O. Lequin, The C-terminal domain of the Uup protein is a DNA-binding coiled coil motif, J. Struct. Biol. 180 (2012) 577–584.
[41] M. Laurence, C. Hatzis, D.E. Brash, Common contaminants in next-generation sequencing that hinder discovery of low-abundance microbes, PLoS One 9 (2014), e97876.
[42] T.C. Maurice, C.E. Mazzucco, C.S. Ramanathan, B.M. Ryan, G.A. Warr, J.W. Puziss, A highly conserved intraspecies homolog of the *Saccharomyces cerevisiae* elongation factor-3 encoded by the HEF3 gene, Yeast 14 (1998) 1105–1113.
[43] A.V. Sarthy, T. McGonigal, J.O. Capobianco, M. Schmidt, S. R. Green, C.M. Moehle, et al., Identification and kinetic analysis of a functional homolog of elongation factor 3, YEF3 in *Saccharomyces cerevisiae*, Yeast 14 (1998) 239–253.

[44] M.J. Marton, C.R. Vazquez de Aldana, H. Qiu, K. Chakraburtty, A.G. Hinnebusch, Evidence that GCN1 and GCN20, translational regulators of GCN4, function on elongating ribosomes in activation of eIF2alpha kinase GCN2, Mol. Cell. Biol. 17 (1997) 4474–4489.
[45] M. Anand, K. Chakraburtty, M.J. Marton, A.G. Hinnebusch, T.G. Kinzy, Functional interactions between yeast translation eukaryotic elongation factor (eEF) 1A and eEF3, J. Biol. Chem. 278 (2003) 6985–6991.
[46] M. Anand, B. Balar, R. Ulloque, S.R. Gross, T.G. Kinzy, Domain and nucleotide dependence of the interaction between *Saccharomyces cerevisiae* translation elongation factors 3 and 1A, J. Biol. Chem. 281 (2006) 32318–32326.
[47] T. Yamada, T. Fukuda, K. Tamura, S. Furukawa, P. Songsri, Expression of the gene encoding a translational elongation factor 3 homolog of Chlorella virus CVK2, Virology 197 (1993) 742–750.
[48] G.C. Atkinson, A. Kuzmenko, I. Chicherin, A. Soosaar, T. Tenson, M. Carr, et al., An evolutionary ratchet leading to loss of elongation factors in eukaryotes, BMC Evol. Biol. 14 (2014) 35.
[49] Y. Inoue, S. Kawai-Noma, A. Koike-Takeshita, H. Taguchi, M. Yoshida, Yeast prion protein New1 can break Sup35 amyloid fibrils into fragments in an ATP-dependent manner, Genes Cells 16 (2011) 545–556.
[50] S. Paytubi, N.A. Morrice, J. Boudeau, C.G. Proud, The N-terminal region of ABC50 interacts with eukaryotic initiation factor eIF2 and is a target for regulatory phosphorylation by CK2, Biochem. J. 409 (2008) 223–231.
[51] A.H. Kachroo, J.M. Laurent, C.M. Yellman, A.G. Meyer, C.O. Wilke, E.M. Marcotte, Evolution. Systematic humanization of yeast genes reveals conserved functions and genetic modularity, Science 348 (2015) 921–925.
[52] B.A. Castilho, R. Shanmugam, R.C. Silva, R. Ramesh, B. M. Himme, E. Sattlegger, Keeping the eIF2 alpha kinase Gcn2 in check, Biochim. Biophys. Acta 2014 (1843) 1948–1968.
[53] T. Hirose, H.R. Horvitz, The translational regulators GCN-1 and ABCF-3 act together to promote apoptosis in *C. elegans*, PLoS Genet. 10 (2014), e1004512.
[54] J. Visweswaraiah, S.J. Lee, A.G. Hinnebusch, E. Sattlegger, Overexpression of eukaryotic translation elongation factor 3 (eEF3) impairs GCN2 activation, J. Biol. Chem. 287 (45) (2012) 37757–37768.
[55] D. Kaida, H. Yashiroda, A. Toh-e, Y. Kikuchi, Yeast Whi2 and Psr1-phosphatase form a complex and regulate STRE-mediated gene expression, Genes Cells 7 (2002) 543–552.
[56] D. Dar, M. Shamir, J.R. Mellin, M. Koutero, N. Stern-Ginossar, P. Cossart, et al., Term-seq reveals abundant ribo-regulation of antibiotics resistance in bacteria, Science 352 (2016), aad9822.
[57] C. Orelle, O. Dalmas, P. Gros, A. Di Pietro, J.M. Jault, The conserved glutamate residue adjacent to the Walker-B motif is the catalytic base for ATP hydrolysis in the ATP-binding cassette transporter BmrA, J. Biol. Chem. 278 (2003) 47002–47008.
[58] P.C. Smith, N. Karpowich, L. Millen, J.E. Moody, J. Rosen, P.J. Thomas, et al., ATP binding to the motor domain from an ABC transporter drives formation of a nucleotide sandwich dimer, Mol. Cell 10 (2002) 139–149.
[59] R.A. Britton, P. Eichenberger, J.E. Gonzalez-Pastor, P. Fawcett, R. Monson, R. Losick, et al., Genome-wide analysis of the stationary-phase sigma factor (sigma-H) regulon of *Bacillus subtilis*, J. Bacteriol. 184 (2002) 4881–4890.
[60] N.C. Shaner, G.G. Lambert, A. Chammas, Y. Ni, P.J. Cranfill, M.A. Baird, et al., A bright monomeric green fluorescent protein derived from *Branchiostoma lanceolatum*, Nat. Methods 10 (2013) 407–409.
[61] P.J. Lewis, A.L. Marston, GFP vectors for controlled expression and dual labelling of protein fusions in *Bacillus subtilis*, Gene 227 (1999) 101–110.
[62] K. Scheinpflug, M. Wenzel, O. Krylova, J.E. Bandow, M. Dathe, H. Strahl, Antimicrobial peptide cWFW kills by combining lipid phase separation with autolysis, Sci. Rep. 7 (2017) 44332.
[63] G. Akanuma, Y. Kazo, K. Tagami, H. Hiraoka, K. Yano, S. Suzuki, et al., Ribosome dimerization is essential for the efficient regrowth of *Bacillus subtilis*, Microbiology 162 (2016) 448–458.
[64] L.V. Schafer, D.H. de Jong, A. Holt, A.J. Rzepiela, A.H. de Vries, B. Poolman, et al., Lipid packing drives the segregation of transmembrane helices into disordered lipid domains in model membranes, Proc. Natl. Acad. Sci. U. S. A. 108 (2011) 1343–1348.
[65] N. Jahn, S. Brantl, H. Strahl, Against the mainstream: the membrane-associated type I toxin BsrG from *Bacillus subtilis* interferes with cell envelope biosynthesis without increasing membrane permeability, Mol. Microbiol. 98 (2015) 651–666.
[66] P.J. Lewis, S.D. Thaker, J. Errington, Compartmentalization of transcription and translation in *Bacillus subtilis*, EMBO J. 19 (2000) 710–718.
[67] A. Sanamrad, F. Persson, E.G. Lundius, D. Fange, A.H. Gynna, J. Elf, Single-particle tracking reveals that free ribosomal subunits are not excluded from the *Escherichia coli* nucleoid, Proc. Natl. Acad. Sci. U. S. A. 111 (2014) 11413–11418.
[68] K.L. Cochrane, Elucidating Ribosomes—Genetic Studies of the ATPase Uup and the Ribosomal Protein L1, University of Michigan, 2015.
[69] M.R. Gibbs, K. Fredrick, Roles of elusive translational GTPases come to light and inform on the process of ribosome biogenesis in bacteria, Mol. Microbiol. 107 (2018) 445–454.
[70] M.A. deLivron, V.L. Robinson, *Salmonella enterica* serovar Typhimurium BipA exhibits two distinct ribosome binding modes, J. Bacteriol. 190 (2008) 5944–5952.
[71] V. Kumar, Y. Chen, R. Ero, T. Ahmed, J. Tan, Z. Li, et al., Structure of BipA in GTP form bound to the ratcheted ribosome, Proc. Natl. Acad. Sci. U. S. A. 112 (2015) 10944–10949.
[72] V. Hauryliuk, G.C. Atkinson, K.S. Murakami, T. Tenson, K. Gerdes, Recent functional insights into the role of (p) ppGpp in bacterial physiology, Nat. Rev. Microbiol. 13 (2015) 298–309.
[73] M.A. deLivron, H.S. Makanji, M.C. Lane, V.L. Robinson, A novel domain in translational GTPase BipA mediates interaction with the 70S ribosome and influences GTP hydrolysis, Biochemistry 48 (2009) 10533–10541.
[74] R.A. Welch, V. Burland, G. Plunkett 3rd, P. Redford, P. Roesch, D. Rasko, et al., Extensive mosaic structure revealed by the complete genome sequence of uropathogenic *Escherichia coli*, Proc. Natl. Acad. Sci. U. S. A. 99 (2002) 17020–17024.
[75] S.N. Cohen, A.C. Chang, Recircularization and autonomous replication of a sheared R-factor DNA segment in *Escherichia coli* transformants, Proc. Natl. Acad. Sci. U. S. A. 70 (1973) 1293–1297.
[76] K.A. Datsenko, B.L. Wanner, One-step inactivation of chromosomal genes in *Escherichia coli* K-12 using PCR products, Proc. Natl. Acad. Sci. U. S. A. 97 (2000) 6640–6645.

[77] F. Grenier, D. Matteau, V. Baby, S. Rodrigue, Complete genome sequence of *Escherichia coli* BW25113, Genome Announc. 2 (2014).
[78] T. Baba, T. Ara, M. Hasegawa, Y. Takai, Y. Okumura, M. Baba, et al., Construction of *Escherichia coli* K-12 in-frame, single-gene knockout mutants: the Keio collection, Mol. Syst. Biol. 2 (2006) (2006 0008).
[79] C. Guthrie, H. Nashimoto, M. Nomura, Structure and function of *E. coli* ribosomes. 8. Cold-sensitive mutants defective in ribosome assembly, Proc. Natl. Acad. Sci. U. S. A. 63 (1969) 384–391.
[80] F.C. Neidhardt, P.L. Bloch, D.F. Smith, Culture medium for enterobacteria, J. Bacteriol. 119 (1974) 736–747.
[81] B. Jia, A.R. Raphenya, B. Alcock, N. Waglechner, P. Guo, K.K. Tsang, et al., CARD 2017: expansion and model-centric curation of the comprehensive antibiotic resistance database, Nucleic Acids Res. 45 (2017) D566-D73.
[82] A.C. Pawlowski, W. Wang, K. Koteva, H.A. Barton, A.G. McArthur, G.D. Wright, A diverse intrinsic antibiotic resistome from a cave bacterium, Nat. Commun. 7 (2016) 13803.
[83] G.B. Mahajan, L. Balachandran, Antibacterial agents from actinomycetes—a review, Front. Biosci. 4 (2012) 240–253.
[84] K. Kadlec, C.F. Pomba, N. Couto, S. Schwarz, Small plasmids carrying vga(A) or vga(C) genes mediate resistance to lincosamides, pleuromutilins and streptogramin A antibiotics in methicillin-resistant *Staphylococcus aureus* ST398 from swine, J. Antimicrob. Chemother. 65 (2010) 2692–2693.
[85] P.E. Douarre, E. Sauvage, C. Poyart, P. Glaser, Host specificity in the diversity and transfer of lsa resistance genes in group B streptococcus, J. Antimicrob. Chemother. 70 (2015) 3205–3213.
[86] J. Lassak, D.N. Wilson, K. Jung, Stall no more at polyproline stretches with the translation elongation factors EF-P and IF-5A, Mol. Microbiol. 99 (2016) 219–235.
[87] S. Ude, J. Lassak, A.L. Starosta, T. Kraxenberger, D.N. Wilson, K. Jung, Translation elongation factor EF-P alleviates ribosome stalling at polyproline stretches, Science 339 (2013) 82–85.
[88] L. Peil, A.L. Starosta, J. Lassak, G.C. Atkinson, K. Virumae, M. Spitzer, et al., Distinct XPPX sequence motifs induce ribosome stalling, which is rescued by the translation elongation factor EF-P, Proc. Natl. Acad. Sci. U. S. A. 110 (2013) 15265–15270.
[89] S. Elgamal, A. Katz, S.J. Hersch, D. Newsom, P. White, W.W. Navarre, et al., EF-P dependent pauses integrate proximal and distal signals during translation, PLoS Genet. 10 (2014), e1004553.
[90] V. Receveur, M. Czjzek, M. Schulein, P. Panine, B. Henrissat, Dimension, shape, and conformational flexibility of a two domain fungal cellulase in solution probed by small angle X-ray scattering, J. Biol. Chem. 277 (2002) 40887–40892.
[91] B. Seip, C.A. Innis, How widespread is metabolite sensing by ribosome-arresting nascent peptides? J. Mol. Biol. 428 (2016) 2217–2227.
[92] K. Kannan, N. Vazquez-Laslop, A.S. Mankin, Selective protein synthesis by ribosomes with a drug-obstructed exit tunnel, Cell 151 (2012) 508–520.
[93] M.M. Almutairi, M.S. Svetlov, D.A. Hansen, N.F. Khabibullina, D. Klepacki, H.Y. Kang, et al., Co-produced natural ketolides methymycin and pikromycin inhibit bacterial growth by preventing synthesis of a limited number of proteins, Nucleic Acids Res. 45 (2017) 9573–9582.
[94] C. Camacho, G. Coulouris, V. Avagyan, N. Ma, J. Papadopoulos, K. Bealer, et al., BLAST+: architecture and applications, BMC Bioinforma. 10 (2009) 421.
[95] A. Stamatakis, RAxML version 8: a tool for phylogenetic analysis and post-analysis of large phylogenies, Bioinformatics 30 (2014) 1312–1313.
[96] M.A. Miller, W. Pfeiffer, T. Schwartz, Creating the CIPRES Science Gateway for Inference of Large Phylogenetic Trees, Gateway Computing Environments Workshop (GCE), New Orleans, LA, 2010 1–8.
[97] T.J. Wheeler, J. Clements, R.D. Finn, Skylign: a tool for creating informative, interactive logos representing sequence alignments and profile hidden Markov models, BMC Bioinforma. 15 (2014) 7.
[98] O. Emanuelsson, S. Brunak, G. von Heijne, H. Nielsen, Locating proteins in the cell using TargetP, SignalP and related tools, Nat. Protoc. 2 (2007) 953–971.
[99] K. Katoh, D.M. Standley, MAFFT multiple sequence alignment software version 7: improvements in performance and usability, Mol. Biol. Evol. 30 (2013) 772–780.
[100] F. Abascal, R. Zardoya, D. Posada, ProtTest: selection of best-fit models of protein evolution, Bioinformatics 21 (2005) 2104–2105.
[101] B.Q. Minh, M.A. Nguyen, A. von Haeseler, Ultrafast approximation for phylogenetic bootstrap, Mol. Biol. Evol. 30 (2013) 1188–1195.
[102] M. Biasini, S. Bienert, A. Waterhouse, K. Arnold, G. Studer, T. Schmidt, et al., SWISS-MODEL: modelling protein tertiary and quaternary structure using evolutionary information, Nucleic Acids Res. 42 (2014) W252–W258.
[103] D. Xu, Y. Zhang, Ab initio protein structure assembly using continuous structure fragments and optimized knowledge-based force field, Proteins 80 (2012) 1715–1735.
[104] L. Schrodinger, The PyMOL Molecular Graphics System, Version 1.8, 2015.
[105] A. Lupas, M. Van Dyke, J. Stock, Predicting coiled coils from protein sequences, Science 252 (1991) 1162–1164.
[106] J. Schindelin, I. Arganda-Carreras, E. Frise, V. Kaynig, M. Longair, T. Pietzsch, et al., Fiji: an open-source platform for biological-image analysis, Nat. Methods 9 (2012) 676–682.
[107] J.D. Te Winkel, D.A. Gray, K.H. Seistrup, L.W. Hamoen, H. Strahl, Analysis of antimicrobial-triggered membrane depolarization using voltage sensitive dyes, Front. Cell Dev. Biol. 4 (2016) 29.
[108] A. Antoun, M.Y. Pavlov, T. Tenson, M.M. Ehrenberg, Ribosome formation from subunits studied by stopped-flow and Rayleigh light scattering, Biol. Proced. Online 6 (2004) 35–54.
[109] A.M. Esposito, T.G. Kinzy, In vivo [35S]-methionine incorporation, Methods Enzymol. 536 (2014) 55–64.